

UNCLASSIFIED

AD NUMBER

ADB024728

LIMITATION CHANGES

TO:

Approved for public release; distribution is unlimited.

FROM:

Distribution authorized to U.S. Gov't. agencies only; Test and Evaluation; SEP 1977. Other requests shall be referred to Air Force Armament Laboratory, Attn: DLDG, Eglin AFB, FL 32542.

AUTHORITY

AFATC ltr, 28 Jan 1981

THIS PAGE IS UNCLASSIFIED

**THIS REPORT HAS BEEN DELIMITED
AND CLEARED FOR PUBLIC RELEASE
UNDER DOD DIRECTIVE 5200.20 AND
NO RESTRICTIONS ARE IMPOSED UPON
ITS USE AND DISCLOSURE.**

DISTRIBUTION STATEMENT A

**APPROVED FOR PUBLIC RELEASE,
DISTRIBUTION UNLIMITED.**

213



AFATL-TR-77-107

BASIC DESIGN ANALYSIS OF GAU-7/A TELESCOPED AMMUNITION

CALSPAN CORPORATION
P. O. BOX 235
BUFFALO, NEW YORK 14221

SEPTEMBER 1977

FINAL REPORT FOR PERIOD
DECEMBER 1975-MARCH 1977

DDC
RECEIVED
FEB 9 1978
F

ADB024728

Distribution limited to U. S. Government agencies only; this report documents test and evaluation; distribution limitation applied September 1977. Other requests for this document must be referred to the Air Force Armament Laboratory (DLDG), Eglin Air Force Base, Florida 32542.

AFB, FL

FILE COPY

AIR FORCE ARMAMENT LABORATORY

AIR FORCE SYSTEMS COMMAND • UNITED STATES AIR FORCE

EGLIN AIR FORCE BASE, FLORIDA



UNCLASSIFIED

SECURITY CLASSIFICATION OF THIS PAGE (When Data Entered)

REPORT DOCUMENTATION PAGE		READ INSTRUCTIONS BEFORE COMPLETING FORM
1 REPORT NUMBER AFATL TR-77-107	2 GOVT ACCESSION NO.	3 RECIPIENT'S CATALOG NUMBER (9)
4 TITLE (and Subtitle) BASIC DESIGN ANALYSIS OF GAU-7/A TELESCOPED AMMUNITION.	5 PERFORMING ORG. REPORT NUMBER AW CALSPAN-VL-5861-D-2	6 TYPE OF REPORT & PERIOD COVERED Final 29 Dec 1975- 31 Mar 1977
7 AUTHOR Edward B. Fisher	8 CONTRACT OR GRANT NUMBER(S)	9 PROGRAM ELEMENT, PROJECT, TASK AREA & WORK UNIT NUMBERS 62602F 2560220 17 Q2
10 PERFORMING ORGANIZATION NAME AND ADDRESS Calspan Corporation P.O. Box 235 Buffalo, New York 14221	11 CONTROLLING OFFICE NAME AND ADDRESS Air Force Armament Laboratory Armament Development and Test Center Eglin Air Force Base, Florida 32542	12 REPORT DATE 14 Sep 1977
13 MONITORING AGENCY NAME & ADDRESS (if different from Controlling Office)	14 SECURITY CLASS. (of this Report) UNCLASSIFIED	15 DECLASSIFICATION DOWNGRADING SCHEDULE
16 DISTRIBUTION STATEMENT (of this Report) Distribution limited to U.S. Government agencies only; this report documents test and evaluation; distribution limitation applied September 1977. Other requests for this document must be referred to the Air Force Armament Laboratory (DLDG), Eglin Air Force Base, Florida 32542.		
17 DISTRIBUTION STATEMENT (of the abstract entered in Block 20, if different from Report)		
18 SUPPLEMENTARY NOTES Available in DDC		
19 KEY WORDS (Continue on reverse side if necessary, and identify by block number) Combustion Mathematical Model Diagnostic Experiments Molded Grain Propellant Heat Transfer Telescoped Ammunition Ignition GAU-7/A		
20 ABSTRACT (Continue on reverse side if necessary and identify by block number) A research program was conducted to determine the causes of variability in GAU-7/A telescoped ammunition featuring molded grain propellant and a combustible case. The approach to the problem took the form of a coordinated analytical/experimental effort. A computer simulation of the GAU-7/A round was formulated, coded, debugged, validated and used to help determine the sensitivity of ammunition parameters. The experimental effort generated empirical inputs and functions for use in the model as		

DDC
 RECEIVED
 FEB 9 1978
 F

DD FORM 1473 1 JAN 73

EDITION OF 1 NOV 65 IS OBSOLETE

UNCLASSIFIED

SECURITY CLASSIFICATION OF THIS PAGE (When Data Entered)

407 727 JOB

UNCLASSIFIED

SECURITY CLASSIFICATION OF THIS PAGE(When Data Entered)

20.

well as defining and providing insight into the variability problem. The results of this program indicate that (1) inconsistent grain breakup (primarily the aft grain), (2) poorly performing and variable ignition components, and (3) interaction of these with a combustible case and other components easily influenced by moisture are primary contributors to GAU-7/A telescoped ammunition performance variability. ↑

UNCLASSIFIED


SECURITY CLASSIFICATION OF THIS PAGE(When Data Entered)

PREFACE

This report, covering the period 29 December 1975 to 31 March 1977 by Calspan Corporation, P.O. Box 235, Buffalo, New York 14221, was performed under Contract No. F08635-76-C-0138 through the Air Force Armament Laboratory, Armament Development and Test Center, Eglin Air Force Base, Florida. Program manager for the Air Force Armament Laboratory was Captain W. Gilliland.

This technical report has been reviewed and is approved for publication.

FOR THE COMMANDER


GERALD P. D'ARCY, Col, USAF
Chief, Guns, Rockets, and Explosives Division

Account for	Section <input type="checkbox"/>
	Section <input type="checkbox"/>
DISCONTINUED	
BY: [Signature]	
DATE: [Date]	
[Large handwritten letter 'B' in a box]	

TABLE OF CONTENTS

<u>Section</u>	<u>Title</u>	<u>Page</u>
I	INTRODUCTION	1
II	COMPUTER SIMULATION DEVELOPMENT	2
	2.1 OVERVIEW	2
	2.2 GAU-7/A DESIGN	3
	2.3 STARTING POINT FOR GAU-7/A SIMULATION	4
	2.4 CODE DESCRIPTION	6
	2.4.1 Code Features	6
	2.4.2 Input Requirements	11
	2.4.3 Limitations	12
III	EMPIRICAL EVALUATIONS	14
	3.1 OVERVIEW	14
	3.2 FIRING TESTS	14
	3.2.1 Test Setup	14
	3.2.2 Tests with As-Received Ammunition	14
	3.2.3 Tests with Conditioned Ammunition	16
	3.2.4 Effects of Primer Strike	16
	3.3 COMPONENT BUILDUP TESTS	19
	3.3.1 Test Setup	19
	3.3.2 Tests and Results	22
	3.3.2.1 Full Rear, Inert Forward Grain Configuration, FRIF	22
	3.3.2.2 Full Rear, Short Forward Grain Configuration, FRSF	28
	3.3.2.3 Full Rear, Medium Forward Grain Configuration, FRMF	28
	3.3.2.4 Medium Rear, Inert Forward Grain Configuration, MRIF	30
	3.3.2.5 Medium Rear, Short Forward Grain Configuration, MRSF	30
	3.3.2.6 Medium Rear, Full Forward Grain Configuration, MRFF	30
	3.3.2.7 Small Rear, Medium Forward Grain Configuration, SRMF	33
	3.3.2.8 Short Rear, Full Forward Grain Configuration, SRFF	33
	3.3.2.9 Primer and Booster Only Configuration	33
	3.3.3 Summary of Significant Observations	35
	3.4 COMBUSTION STUDIES	35
	3.4.1 One-Dimensional Tests	36
	3.4.2 Closed Bomb Tests	38
	3.4.3 Empirical Representations of Molded Grain Combustion	42
	3.5 MISCELLANEOUS TESTS	46
	3.5.1 Propellant Permeability	46
	3.5.2 Propellant Compressive Strength	48
	3.5.3 Projectile Starting Force Tests	49

TABLE OF CONTENTS (CONCLUDED)

<u>Section</u>	<u>Title</u>	<u>Page</u>
IV	COMPUTER SIMULATION STUDIES	54
4.1	OBSERVATIONS	54
4.2	MODEL VALIDATION	54
4.3	PARAMETER SENSITIVITY STUDY	58
4.3.1	Physical Properties	61
4.3.2	Phenomenological Properties	61
4.3.3	Grain Breakup	62
4.3.4	Combustible Cased Ammunition	62
V	CRITIQUE OF GAU-7/A AMMUNITION	63
	REFERENCES	65
APPENDIX	MOLDED GRAIN PROPELLANT POROSITY AND EXPOSED SURFACE AREA	66

LIST OF FIGURES

<u>Figure</u>	<u>Title</u>	<u>Page</u>
1	GAU-7/A Round	3
2	Schematic Diagram of the 105-mm Cartridge Prior to Firing	5
3	Grid Network for Math Model of 25-mm Telescoped Round	8
4	Grid Matrix for the Barrel	10
5	Condition of Screen for Abnormal Shot	17
6	Chamber Pressure and Heating for Shot 23, FRIF	25
7	Chamber Pressure and Heating for Shot 22, FRIF	26
8	Chamber Pressure and Heating for Shot 35, FRIF	27
9	Chamber Pressure and Heating for Shot 27, FRMF	29
10	Chamber Pressure and Heating for Shot 33, MRSF	31
11	Chamber Pressure and Heating for Shot 32, MRFF	32
12	Illustration of the Unsymmetrical and Localized Heating Pattern Generated by the Booster with Inert Fore and Aft Grains	34
13	Comparison of Computed and Experimental Black Powder Combustion Results	39
14	Closed Bomb Test Data - Aft Grain	40
15	Closed Bomb Test Data - Forward Grain	41
16	Burning Area Ratio Versus Chamber Pressure from 200-cc Powder Bomb Tests for Molded Propellant	43
17	Correlation of Burning Surface Area with the Fraction Burned	44
18	Comparison of Experimental Pressure Curve with a Computed Curve Using an Empirical Molded Grain Burn Rate Function	47
19	SEM Photograph of a Molded Grain Exhibiting a Locally Weak Structure	50
20	SEM Photograph of a Molded Grain Exhibiting a Strong Structure	51
21	Comparison of Measured and Computed Pressure Histories Using the Inputs of Table 7	57
22	Comparison of Measured and Computed Pressure Histories	59

LIST OF TABLES

<u>Table</u>	<u>Title</u>	<u>Page</u>
1	FIRING DATA FOR AS-RECEIVED 25-MM TELESCOPED ROUNDS	15
2	FIRING DATA WITH CONDITIONED 25-MM TELESCOPED AMMUNITION	18
3	FIRING DATA WITH VARYING PRIMER STRIKE FORCE	20
4	IDENTIFICATION OF ROUND CONFIGURATIONS	21
5	FIRING TEST DATA	23
6	ONE-DIMENSIONAL CHAMBER TESTS	37
7	TEAM CODE INPUTS FOR VALIDATION CALCULATION	56
8	GAU-7/A PARAMETER SENSITIVITY STUDY	60

SECTION I

INTRODUCTION

The concepts of telescoped ammunition and molded propellant ammunition are both complex and novel in the design of gun systems. Both concepts are employed in the GAU-7/A 25-mm ammunition along with a number of other design innovations.

Telescoped ammunition designs require that the projectile be launched quickly by a booster charge and elements of the main charge in order to obturate the barrel before gas and unburned propellant can escape ahead of the projectile. This sequence of events must occur in a consistent, reproducible manner to assure the degree of reliability and accuracy desired.

Complex ammunition designs of the type under consideration in this program require that the propelling charges be both strong enough to withstand the transporting and chambering forces, yet able to be easily ignited and burned completely. The ignition and combustion sequence must proceed in an orderly and consistent fashion from round to round to minimize performance variations.

This research program represents a coordinated analytical/experimental attempt to determine the causes of the GAU-7/A performance problems. A mathematical model of the GAU-7/A interior ballistics cycle was generated to permit a detailed analysis of the performance of each element of this round. In addition, experimental effort was devoted to determining empirical quantities and relationships for use in the model as well as defining the performance level and variability characteristics of the ammunition components. This coordinated effort has led to identification of sensitive system parameters with suggestions where design improvements can be made.

This report gives the basic elements of the computer model developed and used during this program and a detailed discussion of the experimental effort, sensitivity studies, and a general critique of the ammunition. A detailed description of the code and its use are in Volumes I and II, the Analysts Manual and Users' Manual, Calspan Reports VL-5861-D-3 and VL-5861-D-1.

SECTION II

COMPUTER SIMULATION DEVELOPMENT

2.1 OVERVIEW

Calspan has been involved in mathematical simulation of interior ballistics problems since 1971. At that time, the 81-mm mortar, which is a high-low pressure system with propellant charges in both high and low pressure regions, was modeled. Later, artillery systems were addressed and separate models for the 105-mm howitzer, 155-mm howitzer, 175-mm gun, and 8-inch gun were generated.

These models simulated ignition, flame spread, and combustion of the booster and propellant charge from the time the primer was fired until the projectile passed from the barrel. In each case the propellant was the conventional granular configuration for which combustion is relatively well understood.

The heart of the formulation of these models is the partial differential equations that represent conservation of mass, momentum, and energy in a two-phase, compressible flow system. To this basic element, peripheral calculations of heat transfer, propellant combustion, boundary layer growth, and projectile dynamics are performed. The interior ballistic cycle is simulated with a finite difference technique which incorporates the model formulation into a grid structure. It has been Calspan's philosophy to attempt to model exact gun configurations, which, in many instances, have two and three dimensional phenomena. In the interest of economy, these multi-dimensional effects are represented with multiple one-dimensional, interactive grid networks; that is, mass, momentum, and energy are exchanged between adjacent networks. While not a mathematically rigorous solution, this technique has been demonstrated to create an adequate simulation of complex components while maintaining much of the simplicity, flexibility, and economy of a strictly one-dimensional simulation.

With this background, the task of modeling the GAU-7/A round of ammunition was initiated, clearly the most complex ever attempted. The technology of molded grain propellant is still in a primitive state. Phenomenology of ignition, flame spread, combustion, and eventual grain breakup was not well understood. Designs of molded grain ammunition, especially for the telescoped configuration, have been primarily based on empirical information.

The subject program was initiated in an attempt to upgrade the technology of molded grain-telescoped ammunition through a coordinated analytical/experimental approach. The analytical portion of the program consisted of generating a mathematical simulation of the GAU-7/A ammunition, using Calspan's artillery simulations as the starting point. The experimental effort was devoted to assessing the performance and performance variability of the ammunition components and providing empirical numbers and relationships for use in the simulation. Thus, the computer simulation has become the repository of the technology gained during this program.

This section of the final report will briefly discuss the design of the GAU-7/A ammunition, the starting point of the simulation, and some of the pertinent features and limitations of the code that was generated.

2.2 GAU-7/A DESIGN

The ammunition for the GAU-7/A gun combines several features not found in conventional ammunition. These features include a telescoped projectile, a molded grain propellant charge, and a combustible case. The configuration, shown in Figure 1, consists of an aft molded grain, a forward molded grain that also houses the projectile, a booster charge of black powder, and a primer. The assembly is packaged in a nitrocellulose-fiber container so that the projectile is completely contained. The aft grain contains a hole along the axis which houses the black powder booster and percussion primer. A plastic sleeve separates the booster from the aft grain propellant surface. A retainer ring situated between the molded grains snaps around the projectile base and keeps the projectile stationary. This retainer can withstand a force created by a pressure of 500 psi acting on the projectile base and this provides an initial projectile shot start resistance force.

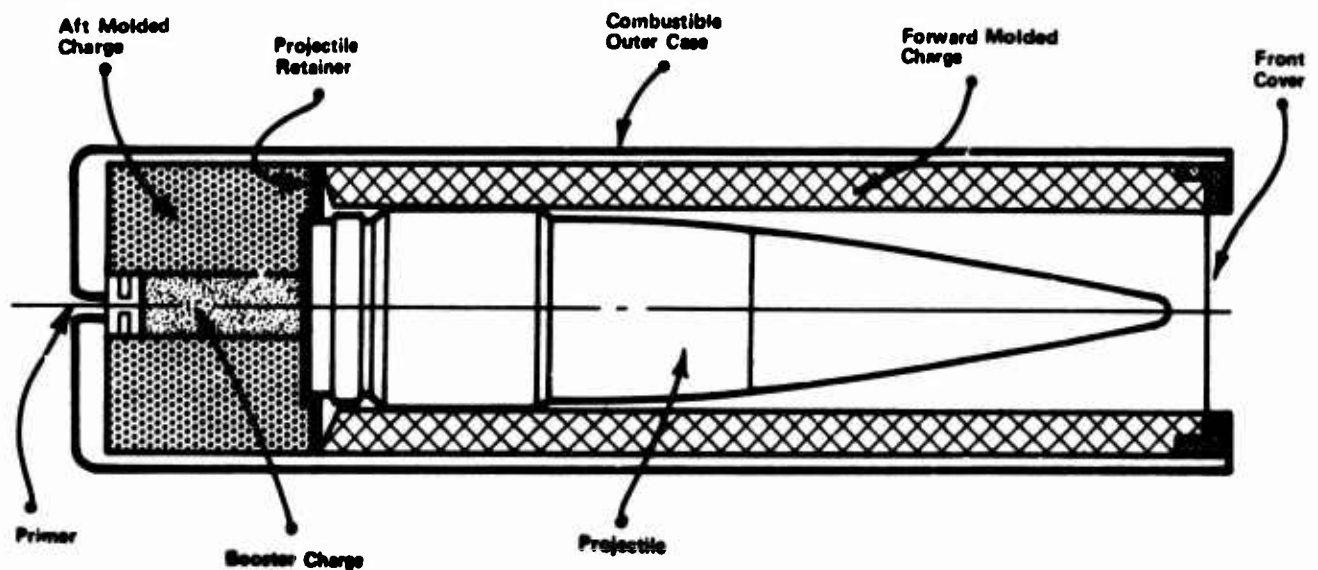


Figure 1. GAU-7/A Round

The firing sequence is initiated when the primer is fired. The primer output ignites the black powder booster. In theory the booster charge is supposed to initiate projectile motion by creating a pressure at the projectile base high enough to cause the retainer to fail. The plastic sleeve separating the booster from the inner surface of the aft grain provides an ignition delay of the aft grain until projectile motion has created some free volume for the burned propellant gas to occupy.

Once the retainer has failed, the projectile experiences practically no resistance until it enters the barrel. As the projectile travels through the forward grain, it exposes grain surface to the hot gas so that it becomes ignited. The aft grain also becomes ignited as a result of deterioration of

and gas flow around the plastic sleeve. When the projectile reaches the barrel, the plastic rotating band is engraved, which causes a substantial increase in projectile resistance force. If the pressure and the projectile momentum are sufficiently high, the projectile will not stop. This is the preferred action.

As propellant combustion proceeds within the molded grains, they become more porous and lose strength. At some point, pressure-induced stresses cause the grains to break up. The loose propellant is then entrained into the barrel, where it burns prior to the time the projectile passes from the barrel.

2.3 STARTING POINT FOR GAU-7/A SIMULATION

The GAU-7/A computer simulation began with the simulation of the 105-mm howitzer, constructed for Picatinny Arsenal on their CDC 6600 computer (Reference 1). The general configuration of 105-mm howitzer ammunition is shown in Figure 2. The complete round consists of a steel cartridge case, primer, propellant charge, and shell. The primer is a long tube with a pattern of holes and is attached to the base of the cartridge case. The tube is initially filled with a charge of black powder which is initiated by firing a percussion-sensitive element. The primer tube has a wax paper liner which allows high pressures to be reached before the tube is vented. The propellant charge consists of seven bags sewn together in a string. Before firing, the projectile is removed and the charge is adjusted by removing bags until the desired velocity level is reached. The first two bags contain 0.0135-inch web single-perf M1 propellant while the remaining five bags contain 0.0245-inch web multiperf M1 powder. The bags are not contoured to fit the case and can be dropped into the case in a random fashion. The charge rests on the bottom of the case and there is considerable free volume between the charge and the projectile. The rotating band performs a sealing function as well as the means for rotational acceleration.

The actual gun system firing sequence as simulated by the 105-mm howitzer code is initiated when the percussion element is fired and causes a sequence of events resulting in black powder ignition. The burning black powder causes the pressure to rise and eventually exceed the strength of the paper liner. Hot gas and burning particles generated by the burning black powder flow through primer tube holes and into the end of the propellant bed. The grains in the main propellant charge are heated by this flow and eventually become ignited. After ignition, the propellant burns at a rate governed by local conditions. Gas flow through the propellant creates forces that result in movement of the bed.

As the pressure builds up in the system, the force created by pressure acting on the projectile base causes it to move, engage the rifling, and eventually overcome the initial barrel restraining force. This restraining force is a result of the material extrusion/shearing phenomena that occur while the rotating band is engraved. When this engraving force has

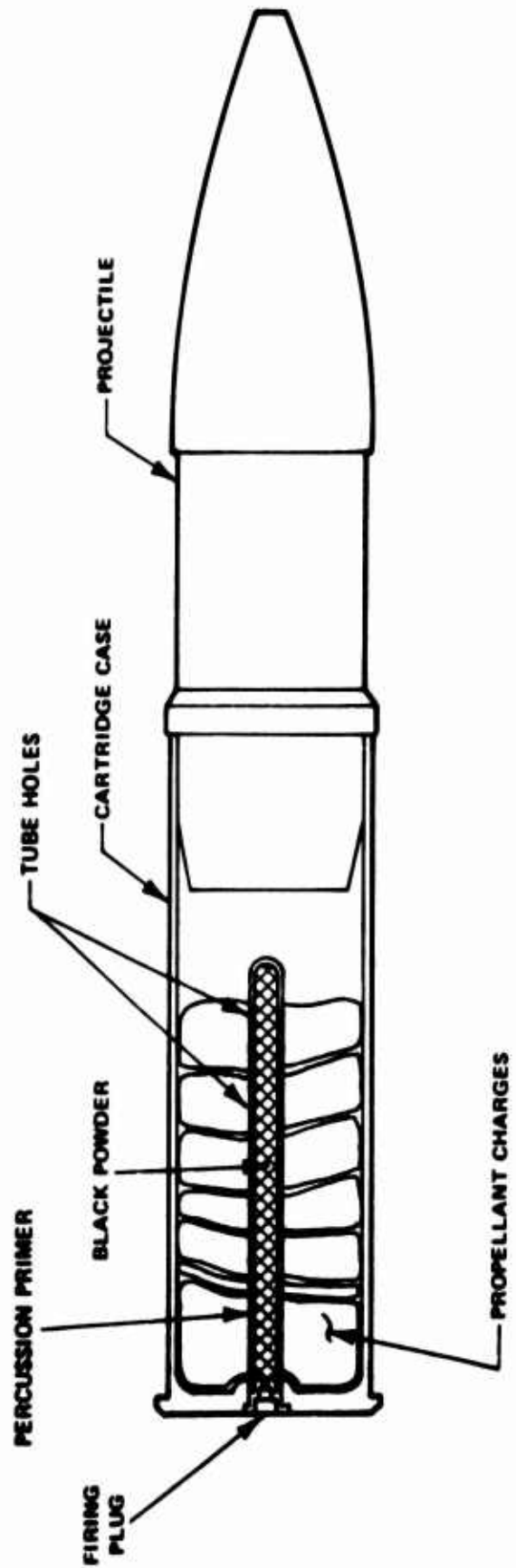


Figure 2. Schematic Diagram of the 105-mm Cartridge Prior to Firing

been exceeded by the pressure, the projectile begins significant acceleration. As the projectile travels through the barrel, it is accelerated in a rotational direction at a rate proportional to the axial acceleration. The 105-mm howitzer considered here has gain twist so that the proportionality parameter varies with projectile travel. This, along with friction and engraving forces, constitutes the projectile retarding forces.

Gas and propellant flow into the barrel behind the moving projectile. The gas loses energy and momentum through the boundary layer while it does work in overcoming the retarding forces. The sequence of events of interest in this model terminates when the projectile has passed from the barrel.

While the 105-mm howitzer and the GAU-7/A appear to have little in common, at first glance, there are certain basic similarities. Both rounds are initiated with a percussion primer and a black powder center core igniter. Propellant also surrounds and is ignited by gas from the center igniter/booster for both rounds. The math model of the 105-mm howitzer contains the necessary one-dimensional representation of black powder combustion, a one-dimensional representation of ignition and combustion of the main propellant charge, and a representation of projectile motion and subsequent flow of gas and propellant grains through the barrel, all essential for certain elements of the GAU-7/A simulation.

2.4 CODE DESCRIPTION

2.4.1 Code Features

The mathematical model consists of three major interconnected routines; aft-chamber, forward-chamber, and barrel. The aft-chamber routine contains the aft portion of the round up to the plastic retainer at the base of the projectile. The forward-chamber routine represents the round from the forward part of the retainer (projectile base) to the forward end of the gun chamber. The barrel routine is responsible for calculating the barrel ballistics.

2.4.1.1 Aft-Chamber Routine

The aft-chamber routine calculates all phenomena concerned with ignition, flame spread, and gas generation and flow in the aft chamber region of the GAU-7/A gun. This region begins with the firing pin and breech seals and continues forward to the plastic projectile retainer. The aft propellant grain, booster, primer, and all facets concerned with initiation are treated in this routine. In addition, flow through close tolerance regions such as between the grain and the fiber case are considered in order to properly conserve mass in the system and to provide a means for calculating heat transfer leading to ignition on all surfaces that come in contact with the flow. The aft portion of the chamber is symmetrical about the axis initially. While three dimensional phenomena occur during a firing, the model assumes that axial symmetry is preserved.

In order to solve the governing equations with a finite difference technique, a grid network was devised to describe the aft portion of the chamber as shown in Figure 3. The matrix consists of:

1. A one-dimensional network to treat ignition, flame spread, and gas flow in the booster, given an empirical primer output.
2. An axisymmetric network to treat ignition, flame spread and gas flow through the aft propellant grain.
3. A one-dimensional network to treat gas flow between the outer surface of the aft grain and the case.

The one-dimensional representation of flow in the booster element is justified on the basis that ignition occurs along a plane and propagates toward the projectile. The axisymmetric representation of the aft propellant grain is deemed necessary because the length to diameter ratio of the aft grain is essentially unity, making radial flame spread propagation nearly as important as axial. In addition, ignition is expected to begin at the base inner surface adjacent to the primer and propagate forward and radially outward with somewhat of a hemispherical flame front. The other network provides a means for calculating gas flow around the outer periphery of the aft grain. Flow parameters from these networks are used to calculate heat transfer and ignition of the surface and interior of the aft grain. When the entire aft grain is ignited and the projectile has moved a short distance, this complex grid structure is not required and the grid system is collapsed into a single one-dimensional network.

These grid networks are not independent but are interconnected in a manner that allows transport of mass, momentum, and energy between adjacent networks. Flow to and from the aft grain is controlled by the low permeability of the grain. Therefore, the pressure drop relationship for flow through a porous medium is used to calculate the flow rate between these matrices.

The GAU-7/A round has a plastic liner that separates the black powder booster from the aft grain. This liner is assumed to prevent radial gas flow through the surface and heating of the propellant covered by it. The extent of this coverage is given through code input parameters. The effects of the liner are assumed to last until pressure in the propellant grain exceeds that in the booster cavity, causing the liner to collapse.

2.4.1.2 Forward-Chamber Routine

The forward-chamber routine contains the projectile, forward propellant grain and considers all events that occur ahead of the projectile retainer. This routine was formulated with three parallel one-dimensional grid networks, as shown in Figure 3, which are:

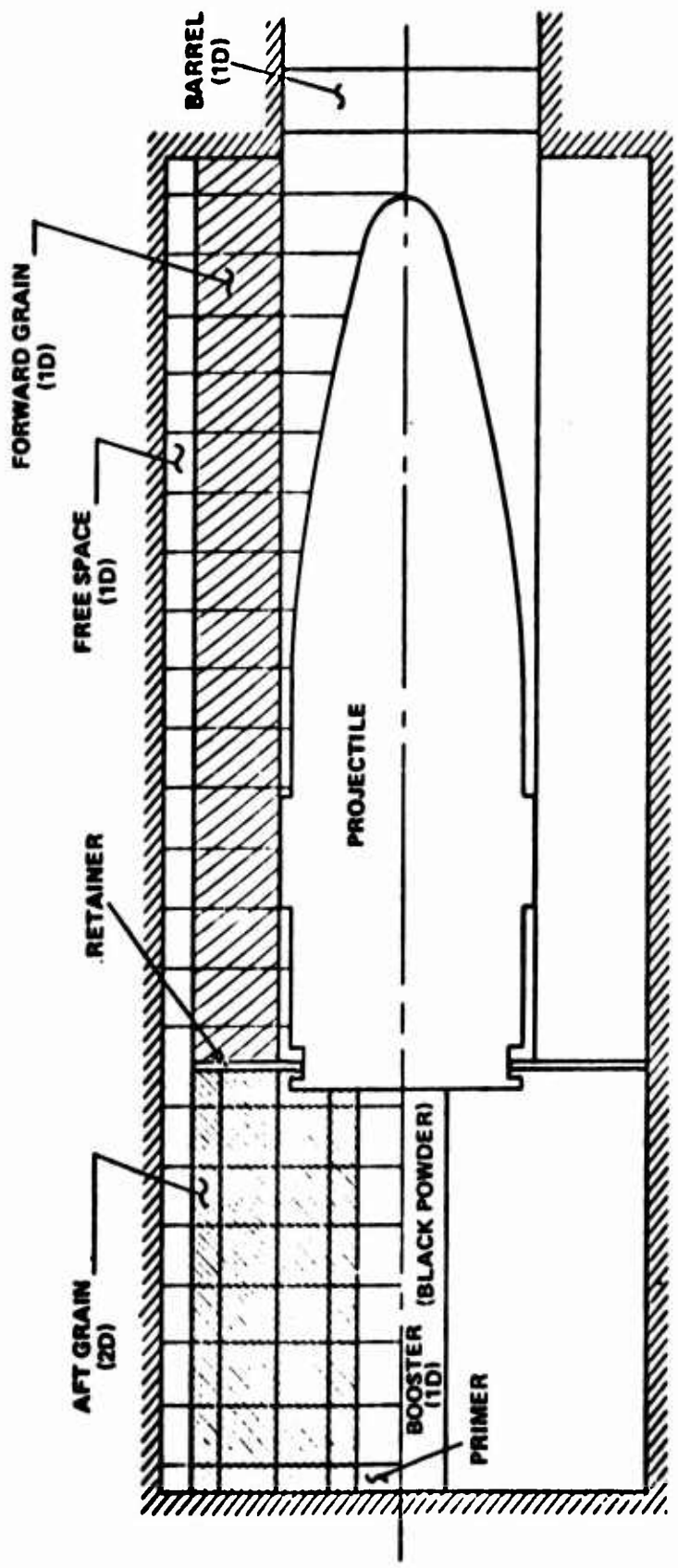


Figure 3. Grid Network for Math Model of 25-mm Telescoped Round

1. A network to describe the region traversed by the projectile.
2. A network to describe the forward propellant grain.
3. A network to describe flow between the forward grain and the case.

One-dimensional grid networks are used here because the radial dimension of any grid system is small in comparison with its length, making axial flow calculations more significant than radial. Differences in flow quantities represented by the parallel grid networks, as influenced by interchange between networks, are considered sufficient to represent radial flow.

When pressure at the projectile base exceeds an input shot start pressure, the plastic retainer fails and the projectile starts to move, allowing gas to be introduced from the aft chamber. Grids are added in the projectile's wake. Special attention was given toward accounting for all gas and unburned propellant that is calculated to pass into the barrel ahead of the projectile, for this is presumed to be a critical event in the firing sequence. This gas is not assumed to cause any significant pressure buildup that would retard projectile motion. When the rotating band reaches the rifling, no flow is allowed ahead of the projectile. At this point, the entire chamber, fore and aft routines, are collapsed into a single one-dimensional grid network. The propellant grains are assumed to be broken at this time because rapid flow of gas into the barrel creates lower pressure on the axis, which tends to promote breakup. At this point, propellant motion calculations are initiated.

2.4.1.3 Barrel Routine

The barrel routine accepts the flow of gas and burning propellant from the chamber and performs the unsteady gas flow and projectile motion calculations until the projectile eventually passes from the barrel. These calculations are performed in a one-dimensional framework which assumes that all two-dimensional effects can be assigned to boundary layer type calculations. The grid network used to represent the barrel is shown in Figure 4.

The one-dimensional equations of fluid motion, modified to take the presence of solid propellant grains into account, are used to calculate the gas flow. These equations express conservation of mass, momentum, and energy for each grid and include losses of momentum and energy as well as the mass flow area constriction due to viscous effects of the boundary layer in the barrel and heat transfer to the barrel wall.

The individual items that influence projectile motion have been accounted for separately rather than being lumped into an effective projectile mass or resistance function. The main propelling force is that due to pressure acting on the projectile base. Retarding forces are considered individually and consist of the force required to engrave the rotating band,

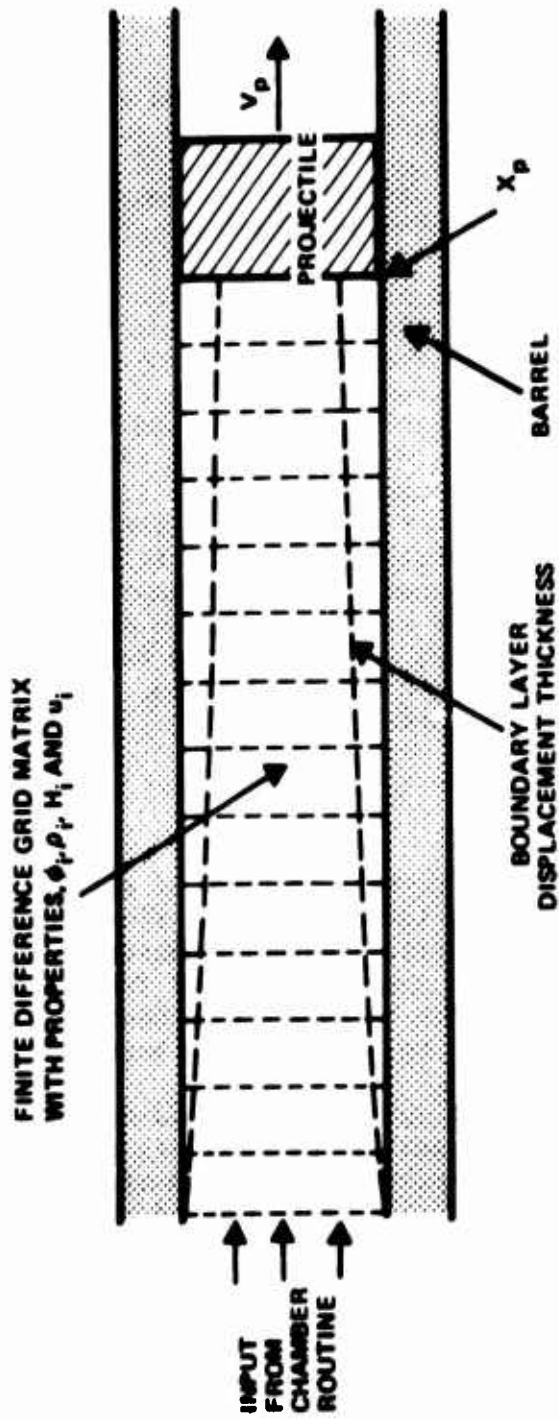


Figure 4. Grid Matrix for the Barrel

the component of the accelerating force consumed by rotational acceleration, and frictional resistance. The engraving force is a result of the extrusion process and subsequent slip fit/galling conditions encountered by the projectile rotating band as it begins motion through the barrel. Rotational acceleration involves the axial moment of inertia and the twist of rifling. It actually becomes a component of the axial acceleration that requires some of the pressure force. In this sense, it acts as a retarding mechanism. The frictional force is assumed to occur as a result of rotational acceleration. The torque required for rotational acceleration is supplied by a resultant force normal to the rifling. The retarding force occurs as a result of the coefficient of friction between the rotating band and the rifling and this resultant normal force.

Barrel routine calculations are initiated when the projectile base has entered the barrel. As pressure causes the projectile to travel through the barrel, grids are added to the network. Initially, a relatively small grid size is required in order to supply the required computational accuracy. As the projectile moves through the barrel, the number of grids becomes excessive and the computational accuracy is greater than required. Therefore, the number of grids in the entire system is cut in half at specified intervals, greatly accelerating the calculation while providing acceptable accuracy.

2.4.2 Input Requirements

The GAU-7/A code is quite input sensitive in that the accuracy of the computed results depends heavily on several empirical input parameters. The most important of these parameters are those that represent propellant linear burn rate and the burning surface area. The linear burn rate, given as $\dot{x} = Bp^n$, is normally obtained from closed bomb testing of propellant used to make the molded grains and can be readily specified.

The burning surface function, for a molded propellant grain, on the other hand, is not well defined and is not a standard measurement for molded propellant. Tests conducted at Calspan, described later in this report, have shown that $A_b = \beta F^n$ is a reasonable approximation of such a function, where F is the fractional amount of propellant burned. This function is included in the code and a reasonable range of values must be provided as code input in order to obtain the desired round performance variation information that variation in this parameter can cause.

The grain permeability is another parameter that has especially unique significance to molded propellant. The rate of gas flow and flame spread through the grain vary with this parameter and so it is quite important. The value of permeability can vary due to variation in density of the molded propellant and the amount of adhesive or binder used. Therefore, values of permeability for a range of molded propellants must be obtained for code input to assess the importance of this parameter.

The remainder of the input requirements include:

1. propellant grain geometric and physical characteristics,
2. propellant ignition temperature and gas properties,
3. projectile retainer failure pressure (shot start),
4. plastic liner coverage,
5. gap between propellant and cartridge case,
6. projectile resistance profile,
7. black powder ignition, combustion and gas characteristics,
8. grid matrix dimensions.

2.4.3 Limitations

The code represents a significant step forward in the ability to design and analyze molded grain telescoped ammunition. However, the GAU-7/A round is extremely complex and there are several limitations and areas where additional effort would be beneficial.

The code formulation, at present, does not contain equations to represent breakup of the molded grains. Calculation of stresses along with specification of failure criteria in terms of strength and strength variability would permit a more accurate assessment of the effects of breakup on round performance. At present, local grain breakup is assumed to occur when the pressure reaches 10,000 psi. This pressure is far in excess of the grain strength and it seems reasonable the pressure difference and gradients experienced by the time the pressure reaches this level ought to be sufficient to make the grain fail structurally. Of course, the code would require more sophisticated inputs if the grain breakup calculation were incorporated. These include a range of grain strength and breakup criteria, depending on how well the granular components of the molded grain adhere to each other.

The code does not consider the phenomena associated with the combustible case. Inclusion of this would require criteria for ignition and a burn rate relationship to be established. This addition would be desirable because the case represents a significant volume of combustible material and is expected to have some influence on round performance and performance variability.

The configuration of the GAU-7/A ammunition allows gas to flow around the extremities of the grains and between the forward aft grains. These leaks represent regions of high flow rate per unit area since there is no restriction other than the size of the hole and boundary layer-type influences. Thus, gas generated by the black powder booster can flow into other regions rather quickly, and cause ignition to occur before the projectile starts to move. These leaks require special treatment in order to be represented adequately, which the present code does not provide.

Projectile retarding forces are never well defined. Dynamic friction forces, engraving forces, and other forces acting on the projectile that tend to slow it down are, for the most part, assumed functions. In the case of telescoped ammunition, gas and unburned propellant can escape into the barrel ahead of the projectile. This can cause excessive pressure buildup ahead of the projectile and add to performance variability. The code allows gas to flow into the barrel ahead of the projectile but it does not use this in the calculation of projectile retarding forces.

Finally, measurements were made to determine the permeability of the molded grain prior to combustion and the effective burn rate during combustion. These experiments, described later in this report, were performed under ideal conditions. It remains to determine the permeability at various stages of combustion and the burning surface area after grain breakup. These are parts of molded grain technology that need further development.

SECTION III
EMPIRICAL EVALUATION

3.1 OVERVIEW

The experimental phase of the program was designed to support two objectives. One was to provide direct insight into the GAU-7/A performance variability problem and to experimentally isolate factors responsible for the variability. The complete round firing tests and modified charge tests fall into this category. The second objective was to provide empirical results to support the mathematical modeling effort. The combustion studies and miscellaneous measurements were performed for this purpose.

3.2 FIRING TESTS

3.2.1 Test Setup

A 25-mm single-shot test fixture designed to fire GAU-7/A ammunition was supplied by Eglin AFB for this program. The fixture was mounted on a steel platform in Calspan's underground gun range, where all firing tests of this program were conducted. Instrumentation for these tests consisted of a single PCB Model No. 119AP pressure transducer mounted in the chamber 0.5 inch from the breech. The pressure data were recorded on an oscilloscope. Muzzle velocity was measured with velocity screens mounted about 15 feet downstream of the muzzle and two Atec counters.

3.2.2 Tests with As-Received Ammunition

The initial firing tests were conducted with GAU-7/A ammunition in the as-received condition, that is, it was not temperature or humidity conditioned or dried before the test. The ammunition was stored at Eglin AFB for several years before being sent to Calspan for these tests. Ammunition lots BWG-24-134 and BWG-24-136 were used for these initial firing tests and the results are tabulated in Table 1.

These tests are characterized by extreme variation and low level of performance, although the variation was less in lot -136 than -134. On successive tests (Runs 10 and 11), the muzzle velocity differed by over 2000 ft/sec and the peak pressure by 13,000 psi.

Variation in unburned propellant blown from the barrel and flash were also observed. The velocity screen nearest the muzzle served as a witness for unburned propellant.

During these tests, the only perforation of the screen for most shots was that made by the projectile. However, each of the screens used

TABLE 1. FIRING DATA FOR AS-RECEIVED 25-MM TELESCOPED ROUNDS

Shot	Muzzle Velocity (fps)	Peak Pressure (psi)	Muzzle Flash	Condition Of First Velocity Screen
1	b	b	Slight	Clean
2	3500	b	Slight	Clean
3	3470	b	Slight	Clean
4	3470	b	Slight	Clean
5	2575	34,000	Yes	Perforated
6	3430	b	Slight	Clean
7	3400	33,500	Slight	Clean
8	1850	27,000	Yes	Perforated
9	3440	33,000	Slight	Clean
10 ^a	1235	24,500	Yes	Perforated
11	3470	37,500	Slight	Clean
12	3490	36,500	Slight	Clean
13	3350	31,000	Slight	Clean
14	3490	36,000	Yes	Clean
15	3585	38,000	No	Clean
16	3410	32,000	No	Clean
17	3490	31,500	No	Clean
18	3610	30,500	Slight	Clean
19	2400	30,500	Yes	Perforated
20	3540	32,000	No	Clean
21	3620	36,000	No	Clean
22	3840	47,000	Yes	Clean
23	3615	35,000	No	Clean
24	3700	38,500	No	Clean

a) The chamber was opened immediately after the shot and several particles of actively smoking material were seen inside.

b) Data are missing due to instrumentation malfunction.

Ammunition Lot BWG-24-134 was used during Runs 1-14.
Ammunition Lot BWG-24-136 was used during Runs 15-24.

for the four shots that exhibited low velocity was perforated all over. (These screens are about 4 1/2 inches x 6 inches in size.) Holes ranged in size from 0.05 inch across to one that was 0.5 inch across, and the 0.05-inch holes predominated. In fact, there were relatively few that were larger. The edges of the smaller holes were cleanly cut and it was very interesting to note that a number of these holes were identical in size and shape to projected outlines of the elemental grains of propellant, i.e., they were either round holes, 0.05 inch in diameter, or rectangular with sides 0.05 inch x 0.07 inch. Sample grid silhouettes are shown in Figure 5 for shot numbers 10 and 11; a perforated screen and a clear one for comparison. The screens for shot numbers 5, 8, and 19 were almost as densely perforated as was the screen for shot number 10.

Severe muzzle flash was also observed during those tests with the lowest muzzle velocity. The fixture was mounted on a platform so that its centerline was located about 5 feet beyond the window in the wall separating the control room and gun area and about 3 feet below the window sill. However, the location of the muzzle station was 5 feet from the right edge of the window. The point to be made by this description is that in order to be readily visible to the observer with ordinary room illumination, the muzzle flash would have to be very bright over a large volume. It was observed to be exceptionally bright during the four low velocity shots.

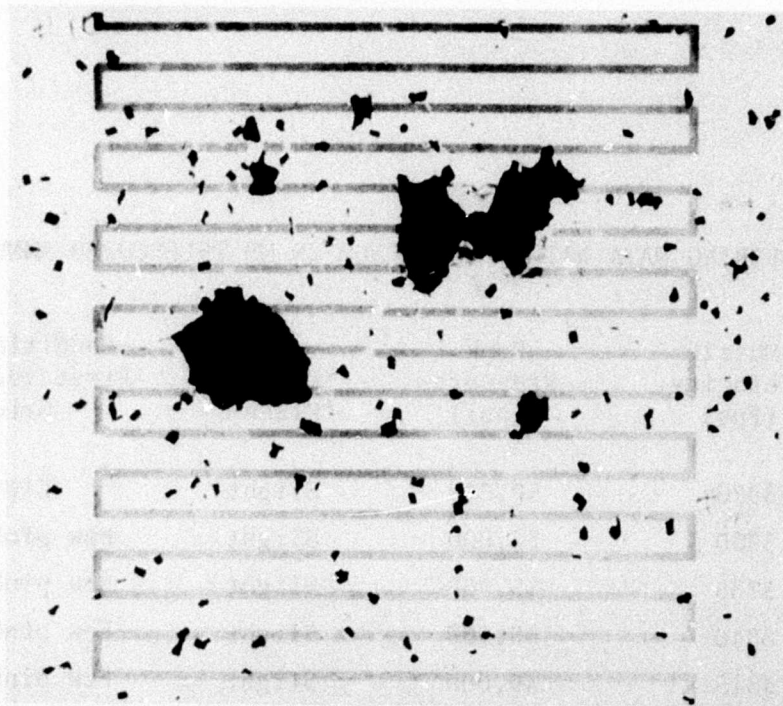
3.2.3 Tests with Conditioned Ammunition

A series of 10 rounds from lot BWG-24-134 were fired after they were oven dried at 128°F for a period of 40 hours and then cooled in a desiccator to room temperature. The results of these tests are shown in Table 2. These rounds exhibited much improved performance and variability characteristics. Peak pressure and muzzle velocity generated during these tests were characteristic of the GAU-7/A round. The difference between these and the as-received rounds vividly demonstrates the adverse effects of moisture resulting from storage in a humid environment.

It is noted that a few pinholes were formed on the velocity screen during several tests. Many rounds had a small amount (a level teaspoon full at most) of loose propellant in the cavity ahead of the projectile. It is surmised that the pinholes were caused by the loose propellant.

3.2.4 Effects of Primer Strike

Late in the program another series of firing tests was conducted with furnace-dried rounds. A pressure transducer was installed at the barrel muzzle for these tests to serve as an indicator of the time the projectile left the barrel. The recording oscilloscope was triggered by a signal from a microswitch actuated by the firing pin as it hit the primer. Therefore, the time the projectile left the barrel, as indicated on the oscilloscope is the action time of the ballistic cycle. The results are



SHOT NO. 10



SHOT NO. 11

Figure 5. Condition of Screen for Abnormal Shot

TABLE 2. FIRING DATA WITH CONDITIONED 25-MM TELESCOPED AMMUNITION

Shot	Muzzle Velocity (fps)	Peak Pressure (psi)	Muzzle Flash	Condition Of First Velocity Grids
1	3970	50,000	Slight	Clean
2	3880	52,000	Slight	Few pinholes ^a
3	3735	55,000	Slight	Few pinholes ^a
4	3840	55,000	Slight	Few pinholes ^a
5	3815	49,000	Slight	Few pinholes ^a
6	3915	52,000	Slight	Clean
7	3825	49,000	Slight	Few pinholes
8	3985	54,500	Slight	Few pinholes
9	3965	58,000	Slight	Clean
10	3915	53,000	Slight	Clean

a) Loose elemental propellant grains could be detected inside the round prior to firing.

shown in Table 3. The column labeled "barrel pressure prior to exit" is that pressure measured at the muzzle end of the barrel before the projectile reached that position.

Surprisingly, the data were quite similar to that obtained from the as-received rounds. The peak pressure and action time exhibited large variability and paper witness panels were hit with a large amount of unburned propellant.

At this point it was observed that the firing pin did not appear to strike the primer with a sharp blow. The firing pin assembly was disassembled and found to be clogged with a tarry substance, which impeded its action. The assembly was cleaned and made to function properly. The final three shots on Table 3 were fired with the hard-striking firing pin and pressure and action time returned to the expected range of performance.

3.3 COMPONENT BUILDUP TESTS

3.3.1 Test Setup

A series of buildup tests was conducted to help experimentally isolate the causes of GAU-7/A performance variability. This type of test involves use of ammunition with various chemically active components of the propellant charge replaced with inert material. The test series began with the primer as the only active component. The component buildup consisted of adding the booster, the aft grain in three stages, and finally the forward grain in three stages. In this way, the performance increment of each addition and the onset of variability could be ascertained.

Eight combinations of inert and active portions of rear and forward grains were assembled as telescoped rounds as described in Table 4 which presents dimensions of rear and forward grains for each combination. Other ammunition components (primer, consumable cases, etc.) were included in each assembly in a condition that was as near the original as possible. Inert portions of the rear grain were made to fit concentrically around live portions of reduced diameter but of full length. Their inside and outside diameters are given by Table 4. Inert portions of the forward grain were made full thickness and to the lengths given by Table 4 in which each represents 1/2 the overall length. The inert portion of the forward grain always was placed forward (towards the muzzle) from the propellant portion and the inert portion of the rear grain was always outside the propellant as indicated earlier. Not indicated on this table are two additional configurations with the primer and the primer-booster the only active components.

The material used for inert portions of the round was particle-board, which is manufactured from wood chips and resin and has approximately the same density, strength, and porosity as the propellant.

TABLE 3. FIRING DATA WITH VARYING PRIMER STRIKE FORCE

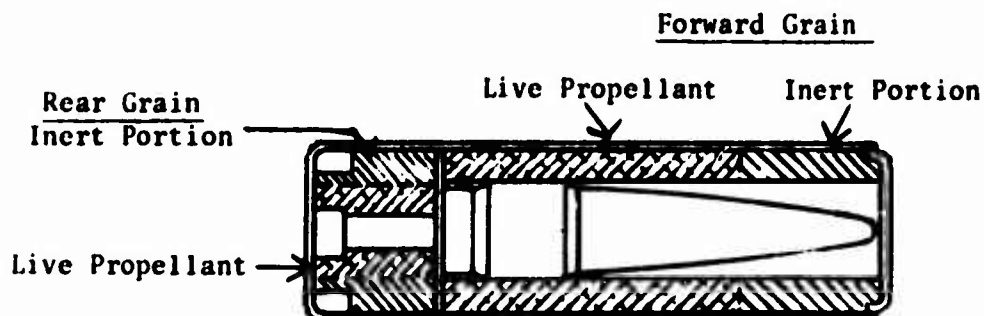
Shot	Pressure (psi)	Barrel Pressure Prior to Exit (psi)	Action Time (msec)	Primer Strike
1	45,000	2900	6.8	Soft
2	31,000	3100	9.9	Soft
3	30,000	2400	8.8	Soft
4	28,000	3600	10.8	Soft
5	42,000	3100	8.1	Soft
6	42,000	200	a	Soft
7	59,000	2000	5.5	Hard
8	62,000	1900	5.1	Hard
9	53,000	700	a	Hard

a) Instrumentation malfunction.

TABLE 4. IDENTIFICATION OF ROUND CONFIGURATIONS

Configuration Designation	Rear Grain Diameters				Forward Grain Length	
	Propellant		Inert		Propellant	Inert
	I.D. (in)	O.D. (in)	I.D. (in)	O.D. (in)	(in)	(in)
SRFF	0.300	0.625	0.625	1.465	4.680	0
SRMF	0.300	0.625	0.625	1.465	3.100	1.580
MRFF	0.300	0.875	0.875	1.465	4.680	0
MRSF	0.300	0.875	0.875	1.465	3.100	1.580
MRIF	0.300	0.875	0.875	1.465	0	4.680
FRMF	0.300	1.465	a	a	3.100	1.580
FRSF	0.300	1.465	a	a	1.560	3.120
FRIF	0.300	1.465	a	a	0	4.680
FRFF	Standard Round					

a) The rear grain of these configurations do not contain inert components.



Helpful keys to understanding the configuration designations:

- SR - small rear grain
- MR - medium rear grain
- FR - full rear grain
- SF - small forward grain
- MF - medium forward grain
- FF - full forward grain
- IF - inert forward grain

The ammunition was fired in the Philco-Ford telescoped-ammunition fixture, which was fitted with a short barrel for most shots (4 inches long). The chamber piece was instrumented with two piezoelectric pressure transducers installed in-line and 1/2 inch from either end. Two chromel-alumel thermocouple-equipped heat sensors were installed at the same stations as the pressure transducers such that their end faces were flush with the chamber wall. Muzzle velocity was measured and movies were taken at the muzzle during five of the shots. The ammunition was oven-dried at 140°F for at least 24 hours previous to all shots.

After firing several shots using standard rounds to check instruments and recording devices, the recording arrangement was fixed except that sensitivities were changed depending upon the potency of the round. One dual-beam oscilloscope was used for recording the two heat-sensor traces and it was triggered by a microswitch in a dry-cell circuit that was tripped by motion of the gun trigger. Two dual-beam oscilloscopes were used to record pressure. Each recorded both transducer outputs. One was triggered by the microswitch circuit mentioned above and the other by the pressure signal so that it usually was triggered later than the other.

3.3.2 Tests and Results

Test data are presented in Table 5. The data include peak pressures, duration of raised chamber pressure, and timing of various events, such as time to reach 750 psig at the breech, time to reach peak pressure, time to start increase of chamber pressure at both the breech end and barrel end, and time to initial temperature rise of heat sensors at both ends of the chamber. Muzzle velocity was included but it is suspected that, for some rounds, debris cut the first screen before the projectile.

These data have yielded a number of observations and conclusions. First, these will be discussed for each specific configuration of the modified round.

3.3.2.1 Full Rear, Inert Forward Grain Configuration, FRIF

The barrel-end heat sensor displayed a wide range of response and intensity of heating, varying from zero delay for shot number 22 to 16 msec for number 23. Heating was low for shot 23 and intense for 24 and 36. The rate of heating was generally highest while pressure was high at the barrel end. At the breech end, variability of response and heat intensity was also indicated but heating started at or before pressure started to rise. Very intense breech-end heating was indicated for shots 23, 24, and 36, i.e., which was not always consistent with barrel-end heating for all shots, e.g., number 23. Response was immediate for 23 and 24 even though their pressure rise was very late.

TABLE 5. FIRING TEST DATA

SHOT	COMPO. VARIATION	TIME ¹ TO PEAK PRESSURE AT START > 750 (msec)	TIME ² TO PEAK PRESSURE AT BREACH (msec)	TIME ³ TO INITIAL PRESSURE RISE AT BREACH (msec)	BREACH PRESSURE AFTER INITIAL PRESSURE RISE (psi)	TIME ⁴ TO INITIAL TEMPERATURE RISE (msec)		PEAK BREACH PRESSURE (psi)	DURATION OF PRESSURE TRACE (msec)	RESIDUE	COMMENTS
						AT BREACH	AT BARREL				
9	PRPF	PRESSURE AT START > 750	3.0	1.4	1.4	2770	1	0	7	NONE	STD ROUND
10	PRPF	PRESSURE AT START > 750	3.4	1.0	1.4	1800 ^c	0 ^c	1.3	3.0	NONE	STD ROUND
21	PRPF	PRESSURE AT START > 750	7	7	7	NO JUMP	7	7	4.5	NONE	STD ROUND
14	PRPF	PRESSURE AT START > 750	5.7	3.5	2.4	2000	2.0 ^c	3.0	> 5	9% OF CASE LEFT WELL CHARR'D	
20	PRPF	2.3	4.3	2.3	2000	2000	1.0	7	6.0	VERY LITTLE	FILMED
26	PRPF	1	6.0	0	NO JUMP	NO JUMP	BEFORE 1-0	3.0	6.0	NONE	
26	PRPF	7	7	7	NO JUMP	NO JUMP	0 ^c	0 ^c	6.0	NONE	
27	PRPF	0.4	4.0	PRESSURE WAS UP AT 1-0	1300	1300	0 ^c	0 ^c	6.0	VERY LITTLE	
13	PRPF	2.2	4.0	1.0	NO JUMP	NO JUMP	0	5.0	6.0	COMPLETE CASE LEFT WELL CHARR'D AND SPLIT FULL LENGTH	
17	PRPF	0.3 msec BEFORE PEAK	7	7	NO JUMP	NO JUMP	7	7	6.0	2/3 CASE LEFT PARTIALLY CHARR'D SPLIT FULL LENGTH	FILMED
25	PRPF	0.3	6.0	3.0	1200	1200	3.0 ^c	4.0	6.0	LARGE PIECE OF INERT CHARGE LEFT	
20	PRPF	0.5	3.0	0.5	1200	1200	2.0 ^c	4.0 ^c	5.5	SMALL PIECE OF CHARR'D CASE LEFT	
24	PRPF	PRESSURE AT START > 750	4.0	PRESSURE WAS UP AT 1-0	NO JUMP	NO JUMP	0 ^c	4.0	> 10		
10	PRPF	0.3 msec BEFORE PEAK	7	5 msec AFTER BREACH	NO JUMP	NO JUMP	0	7	> 6	CASE LEFT BUT WAS ONLY A WEAK CHAR SPLIT FULL LENGTH	LONG BARREL PRESSURE TRACE STOPPED BEFORE IT RETURNED TO ZERO
11	PRPF	0.5	15.0	0.0	NO JUMP	NO JUMP	0	7	> 7	CHARR'D CASE LEFT AND 3/4" LONG RING OF INERT CHARGE	LONG BARREL PRESSURE TRACE STOPPED BEFORE IT RETURNED TO ZERO
12	PRPF	5.5	11.0	3.5	NO JUMP	NO JUMP	7	7	> 8	SCORCHED CASE AND FORWARD GRAIN LEFT	LONG BARREL
16	PRPF	0.0	6.5	1.0	NO JUMP	NO JUMP	7	1.0	> 10	WELL CHARR'D SPLIT BUT COMPLETE CASE LEFT	FILMED
22	PRPF	2.0	6.0	0	1200	1200	0	0	16.0	NONE	
23	PRPF	12.0	10.0	0	NO JUMP	NO JUMP	0.4	17.0	11.0 ^c	NONE	
24	PRPF	10.0	14.0	7	NO JUMP	NO JUMP	~ 2.0	4.0 ^c	11.0	NONE	
25	PRPF	PRESSURE AT START > 750	3.5	UP AT 1-0	NO JUMP	NO JUMP	0	2.0	26.0	FORWARD GAIN AND CASE LEFT BUT CHARR'D	LONG BARREL
26	PRPF	0.1	3.4	0 ^c	1400	1400	~ 1.0	4.0	16.0	FEW PIECES OF CASE LEFT	LONG BARREL
22	SRPF	2.2 ^c	5.0	0	1400	1400	0	4.0	7.0 ^c	NONE	
20	SRPF	0.0	11.0	0	1400	1400	0	2.5	16.0	INERT FORWARD GAIN LEFT	
10	SRPF	0.5 msec BEFORE PEAK	7	7	1400	1400	BEFORE 1-0	3.0	5.0	VERY LITTLE	
10	SRPF	7	7	7	1400	1400	0	3.0 ^c	7	1/3 OF FORWARD INERT GRAIN LEFT	FILMED
20	SRPF	7	7	> 8	1400	1400	BEFORE 1-0	4.0	7	NONE	
31	SRPF	0.3 msec BEFORE PEAK	7	7	1400	1400	SAME AS AT BREACH	1.0	12.0	VERY LITTLE	

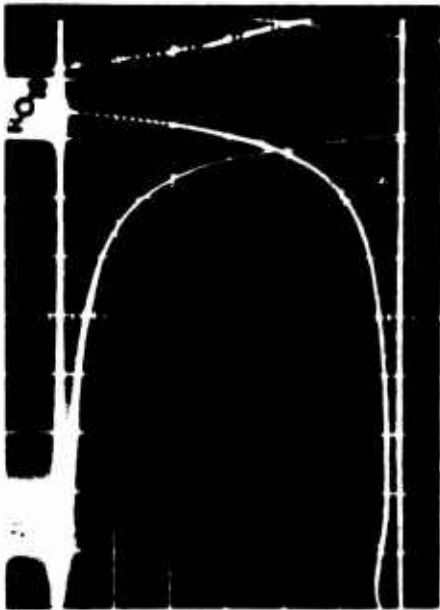
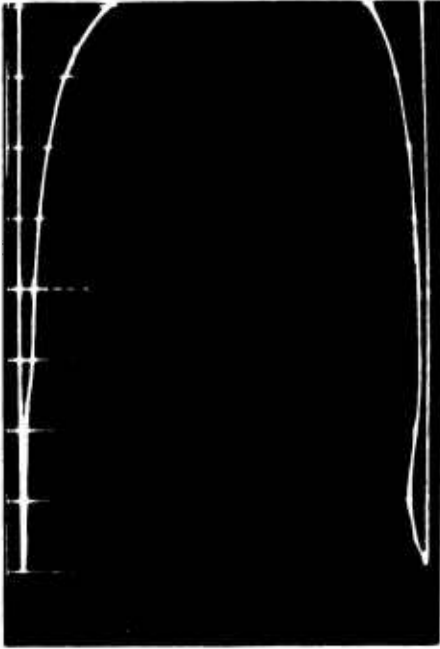
¹TIME FROM BREACH SWITCH CLOSURE
²BARREL PRESSURE IS ABOVE ZERO BY 10% OF PEAK VALUE
³PRECISION IS POOR

An interesting phenomenon that was detected for shots 23 and 24 was a pressure "bump" that occurred well before the climb to peak pressure. The breech-end pressure trace for shot 23 (Figure 6) shows an immediate rise to a low level and a decrease to almost zero again in 5 msec. The pressure does not climb again until much later, in fact it is 11 msec before it reaches the peak level of the "bump" again, which may not be sufficiently high to effectively start the projectile. Nevertheless, heating at the breech end starts at time zero and persists at least until the pressure peaks. (Heating rate is proportional to the slope of these temperature traces.) Shot 24 shows the same kind of bump but less delay before the subsequent rise to peak pressure. The highest peak pressures for this configuration were exhibited by shots 23 and 24, which also exhibited longest time to peak pressure. By contrast, the pressure traces for shot 22 were completely different (Figure 7) and heating rates were relatively low at both ends of the chamber. This shot produced a low peak-chamber pressure, 2600 psi. Pressure was starting to climb when scopes were triggered, which was at the time heating started at both ends. At 2 msec, the breech pressure suddenly jumped as if the pressure tap became cleared.

A much smoother breech-end pressure trace was exhibited for shot 35 which peaked at 2800 psi, about the same as for shot 22 (Figure 8). Heating rates are similar for both shots. However, for this shot it was the barrel-end pressure trace that suddenly jumped exhibiting almost a step change from practically zero gage pressure to almost peak pressure. Even so, the two pressure traces of shot 35 peaked simultaneously whereas during shot 22 the barrel end pressure peaked almost 2 msec later than did the breech-end trace, which peaked after steadily climbing at a modest rate.

An aluminum sting was attached to the projectile nose for shot 16 and the shot was filmed at 20,000 pps. The sting was 7 inches long, 1/4 inch in diameter at its base, and tapered so that it was about 1/8 inch at the tip. It was painted in 1 inch long bands alternately orange and white. At the start of filming about 1/2 inch of the sting projected from the muzzle into camera view. The first motion visible on the film is that of the tip of the sting. After it moves 1 1/2 inches, a puff of smoke or fine debris (too fine to distinguish particles) appeared and spurted past the sting, obscuring it. When it cleared, the sting had travelled several inches and was moving. As the projectile rotating band cleared the muzzle, a dark cloud of smoke overtook the projectile, obscuring it completely. The breech pressure trace showed a long period (5 msec) while pressure slowly climbed at an almost constant rate of 200 psi/msec. Then, after climbing at an accelerating rate, it peaked at only 1500 psi, whereupon it dropped to about 800 psi and persisted there for 6 msec before slowly dropping off.

Apparently, ignition of the rear grain is very inconsistent. The initially-generated gases from both primer and black powder flow outside the case at the breech end but affect the chamber wall and case at the barrel end only slightly. This was especially evident for shots 23 and 24 that exhibited what appeared to be a considerable delay in the ignition of black powder.

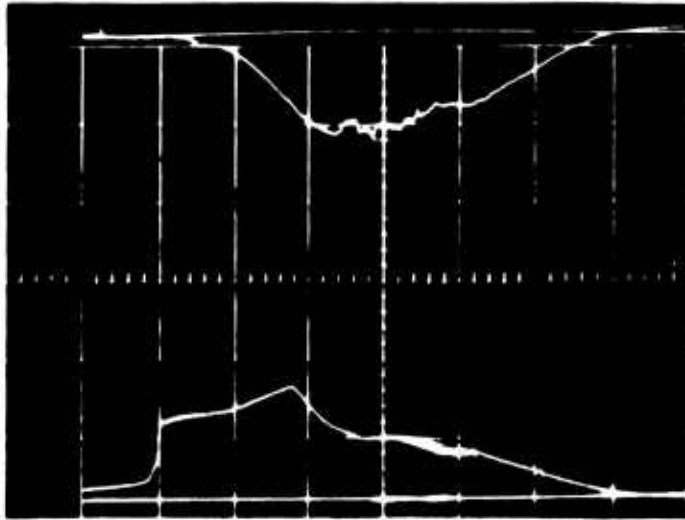


UPPER TRACES ~ BARREL-END CHAMBER PRESSURE, 200 psi/div, 2 msec/div
 LOWER TRACES ~ BREECH-END CHAMBER PRESSURE, 1000 psi/div, 2 msec/div
 LEFT PICTURE - TRACES TRIGGERED BY PRESSURE

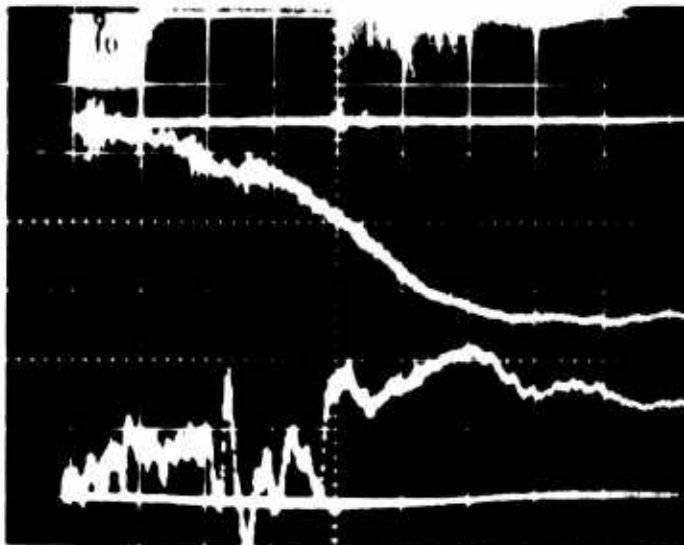


UPPER TRACE ~ BARREL-END CHAMBER-WALL TEMPERATURE } 22° F/div, 2 msec/div
 LOWER TRACE ~ BREECH-END CHAMBER-WALL TEMPERATURE }
 TRACES TRIGGERED BY MICROSWITCH

Figure 6. Chamber Pressure and Heating for Shot 25, FRIF

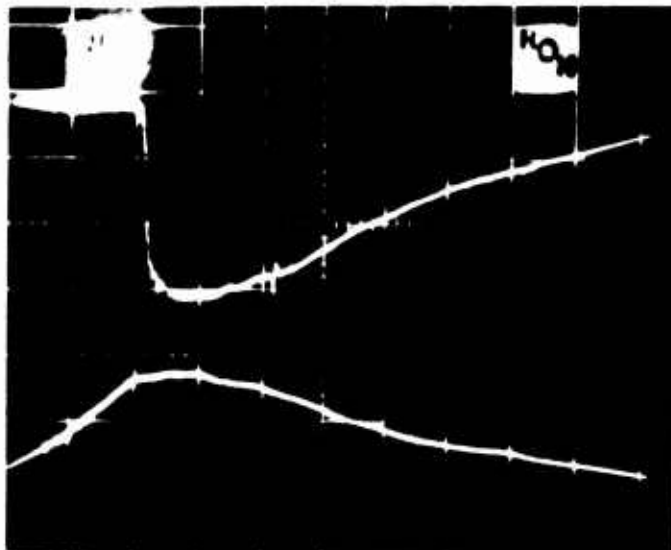


UPPER TRACE ~ BARREL-END CHAMBER PRESSURE, 200 psi/div, 2 msec/div
 LOWER TRACE ~ BREECH-END CHAMBER PRESSURE, 1625 psi/div, 2 msec/div
 TRACES TRIGGERED BY MICROSWITCH

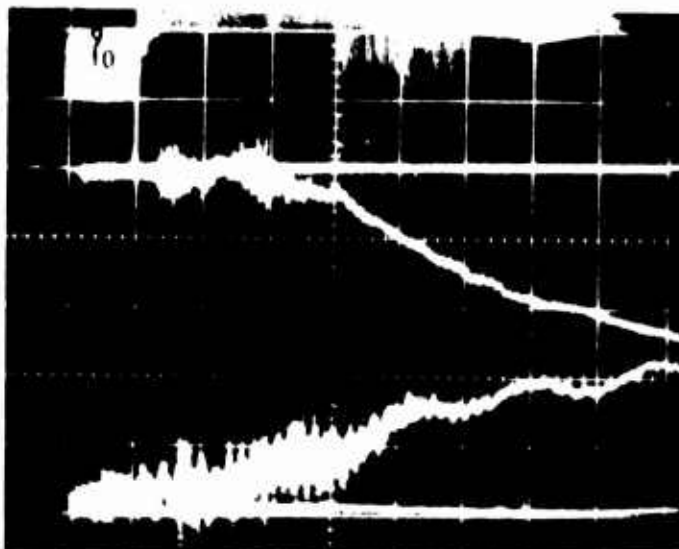


UPPER TRACE ~ BARREL-END CHAMBER-WALL TEMPERATURE } 22°F/div, 2 msec/div
 LOWER TRACE ~ BREECH-END CHAMBER-WALL TEMPERATURE }
 TRACES TRIGGERED BY MICROSWITCH

Figure 7. Chamber Pressure and Heating for Shot 22, FRIF



UPPER TRACE ~ BARREL-END CHAMBER PRESSURE, 200 psi/div, 0.5 msec/div
 LOWER TRACE ~ BREECH-END CHAMBER PRESSURE, 1625 psi/div, 0.5 msec/div
 TRACES TRIGGERED BY PRESSURE



UPPER TRACE ~ BARREL-END CHAMBER-WALL TEMPERATURE } 22°F/div, 0.5 msec/div
 LOWER TRACE ~ BREECH-END CHAMBER-WALL TEMPERATURE }
 TRACES TRIGGERED BY MICROSWITCH

Figure 8. Chamber Pressure and Heating for Shot 35, FRIF

3.3.2.2 Full Rear, Short Forward Grain Configuration, FRSF

Records for these shots showed that the start of barrel-end heating was somewhat delayed and reached only moderate levels, the hottest one being the shot that exhibited the lowest peak pressure, 28. Heating at the breech end started before the barrel-end heating and was moderate, about the same for 3 shots (28, 29, and 34) and slightly higher for 13. No general statement can be made relating heating and pressure histories, but the heating did appear to be highest during the period of falling chamber pressure for both ends of the chamber.

Shot 17 was filmed. The first movement that can be seen is of the sting. When it advances 3 inches a puff of smoke is ejected past it, but it is not completely obscured. As the view clears, the sting moves out farther until large volumes of gas and smoke are released and the sting is obscured. At no time while the sting was in view could it be seen to hesitate.

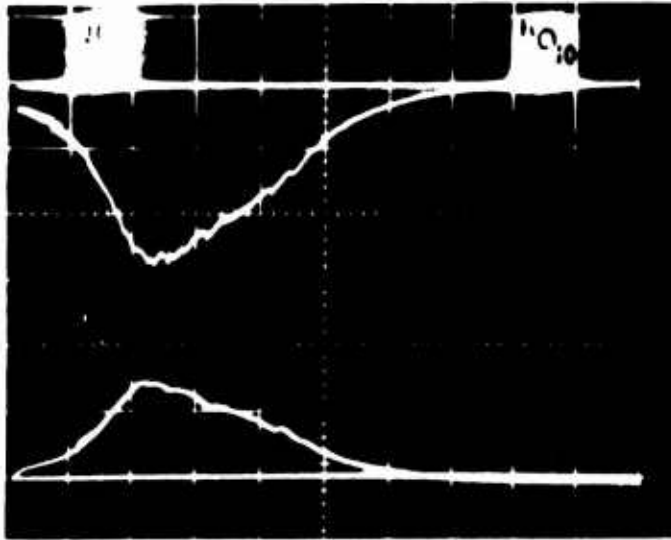
Variations in pressure and heating levels were not extreme for this configuration but the periods of raised pressure varied from 8 to more than 16 msec. Therefore, it cannot be concluded that the provision of some propellant forward from the rear grain produced any benefits.

3.3.2.3 Full Rear, Medium Forward Grain Configuration, FRMF

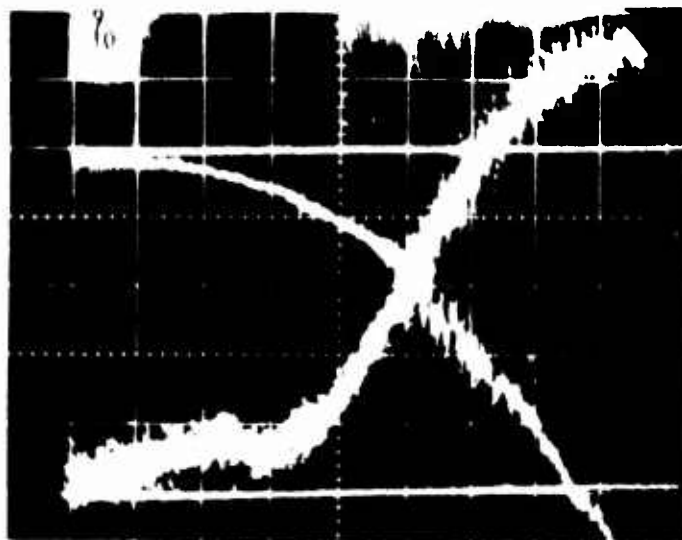
Intensity of heating varied widely at both ends of the chamber. At the barrel end, heating increased rapidly as soon as the chamber pressure started to fall whereas at the breech end, heating rose rapidly only after pressure was well down past its peak.

Shot 20 was filmed at 17,500 pps which yielded much brighter, clearer images. First motion was of the sting, and it had moved only 1 inch in 1.6 msec when it was obscured by a dark puff of smoke in which no particles could be discerned. When the view cleared the sting was out 6 inches at about 2.6 msec and moving. At 3.1 msec the tip of the projectile appeared and in two more frames smoke and gas was released when the rotating band cleared the muzzle, which again obscured the projectile. When the view started to clear again only a few chunks or particles could be seen.

This configuration was generally the most consistent performer of all the modified rounds. Pressure traces were similar if not always peaking at the same value, and the heat sensor traces that were obtained showed similar effects. Typical oscilloscope records are shown in Figure 9. It appears that the rear portion of the forward grain is very effective and tends to partially compensate for the poor performance of the rear grain.



UPPER TRACE ~ BARREL-END CHAMBER PRESSURE, 1000 psi/div, 1 msec/div
 LOWER TRACE ~ BREECH-END CHAMBER PRESSURE, 8130 psi/div, 1 msec/div
 TRACES TRIGGERED BY PRESSURE



UPPER TRACE ~ BARREL-END CHAMBER-WALL TEMPERATURE, 44°F/div, 1 msec/div
 LOWER TRACE ~ BREECH-END CHAMBER-WALL TEMPERATURE, 44°F/div, 1 msec/div
 TRACES TRIGGERED BY MICROSWITCH

Figure 9. Chamber Pressure and Heating for Shot 27, FRMF

3.3.2.4 Medium Rear, Inert Forward Grain Configuration, MRIF

Heating at both ends of the chamber was very low. At the muzzle end it increased with chamber pressure. Only the beginning of a pressure trace was obtained for shot 19 because of the prolonged period of raised pressure which was greater than the oscilloscope sweep time. This was unfortunate because this shot was filmed. However, a pressure trace was obtained for shot 18, which exhibited similar characteristics, such as heating. The camera operated at about 17,000 pps. The film showed that at start, 1/2 inch of the sting was in view and first motion was of the sting. At 4.9 msec, it reached a 2-inch extension and a puff of smoke was ejected past it. This had a well-defined front of nearly spherical shape approximately 4 inches in radius. In 0.65 msec it had moved 1 inch farther. In 0.53 msec, it moved another inch and a third inch was traveled in another 0.53 msec (157 fps), when it came to a stop with 5 inches showing. Then it waved back and forth in 4 complete oscillations before it started moving forward again, 15.7 msec after stopping. It was out to 6 inches in 0.16 msec after motion restarted, 7 inches 0.12 msec later (projectile nose at muzzle) (694 fps), and in 0.17 msec more, 2 inches of projectile nose was showing (980 fps). In the next frame, dark smoke appeared that persisted for a relatively long time. As it dispersed, numerous large pea-sized pieces of debris could be seen leaving the muzzle.

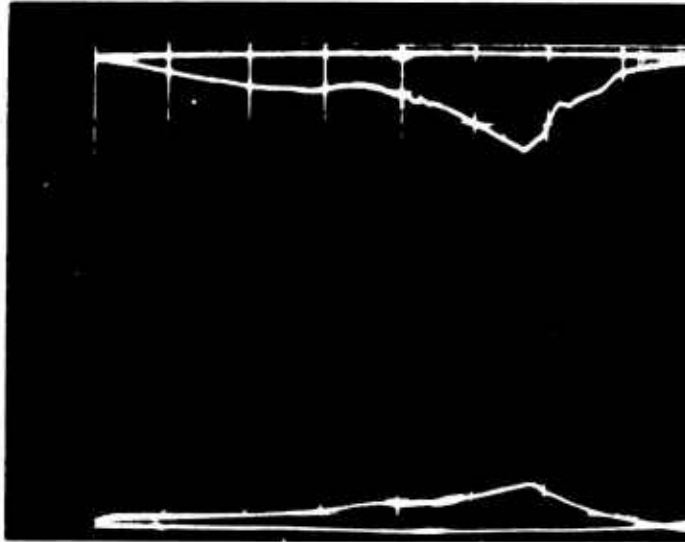
3.3.2.5 Medium Rear, Short Forward Grain Configuration, MRSF

Only one shot (33) was fired of this configuration but good data were obtained. The pressure trace peaked almost sharply instead of the rounded hump shown by shot 18 (MRIF) as can be seen from Figure 10. The heating rate at the breech end was very high from the start which coincided with the beginning of the pressure rise. The heating rate decreased slightly after 4 msec, but pressure did not peak until after 11.5 msec.

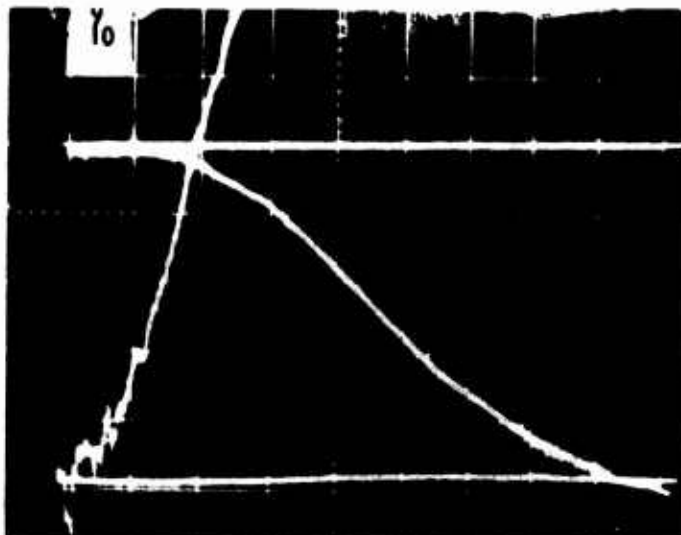
At the barrel end of the chamber, the heating rate was moderately high and peaked while pressure was in its second stage of climb. After the pressure peaked heating rate dropped, with a definite change apparent at the time of the peak.

3.3.2.6 Medium Rear, Full Forward Grain Configuration, MRFF

Only one shot of this configuration was fired but again good traces were obtained and are shown by Figure 11. Pressure traces are more typical of a gun except that considerable delay in pressure rise can be seen (3 msec). On the other hand, breech end heating started up immediately as if signalled by the triggering of the scope. Its intensity decreased until peak pressure was reached whereupon it increased again.

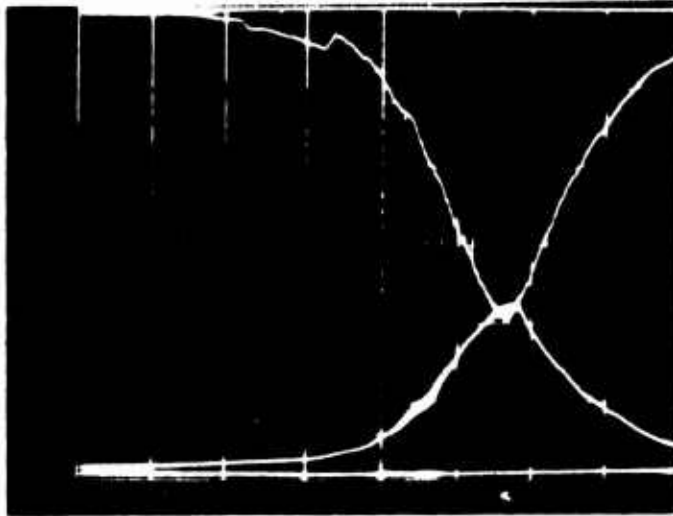


UPPER TRACE ~ BARREL-END CHAMBER PRESSURE, 200 psi/div, 2 msec/div
 LOWER TRACE ~ BREECH-END CHAMBER PRESSURE, 1625 psi/div, 2 msec/div
 TRACES TRIGGERED BY MICROSWITCH

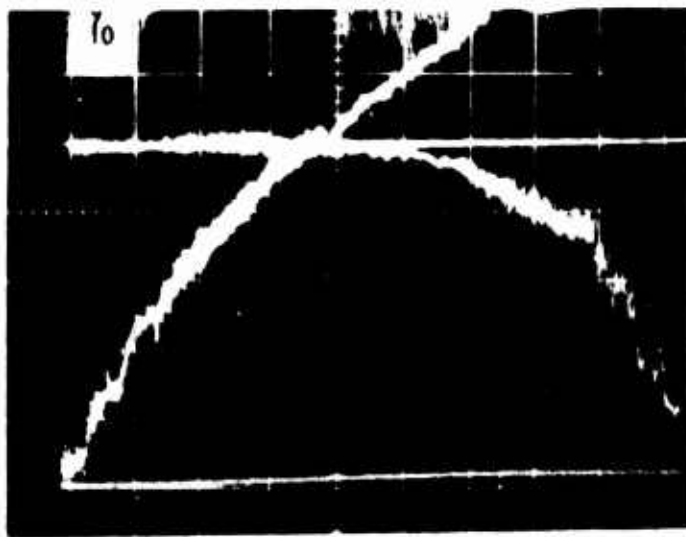


UPPER TRACE ~ BARREL-END CHAMBER-WALL TEMPERATURE } 22°F/sec, 2 msec/div
 LOWER TRACE ~ BREECH-END CHAMBER-WALL TEMPERATURE }
 TRACES TRIGGERED BY MICROSWITCH

Figure 10. Chamber Pressure and Heating for Shot 33, MRSF



UPPER TRACE ~ BARREL-END CHAMBER PRESSURE, 1000 psi/div, 1 msec/div
 LOWER TRACE ~ BREECH-END CHAMBER PRESSURE, 8130 psi/div, 1 msec/div
 TRACES TRIGGERED BY MICROSWITCH



UPPER TRACE ~ BARREL-END CHAMBER-WALL TEMPERATURE } 22°F/msec, 1 msec/div
 LOWER TRACE ~ BREECH-END CHAMBER-WALL TEMPERATURE }
 TRACES TRIGGERED BY MICROSWITCH

Figure 11. Chamber Pressure and Heating for Shot 32, MRFF

At the barrel end there was almost no heating until the pressure peaked. Then it increased rapidly and reached a maximum when pressure had dropped to 15 percent of peak.

3.3.2.7 Small Rear, Medium Forward Grain Configuration, SRMF

Heating rates started immediately upon triggering at the breech end and 3 msec later at the barrel end and both continued at a constant, moderate rate. No relation between heating and pressure was indicated. Both pressures peaked sharply, almost simultaneously. Their traces were very similar to those of shot 33, Figure 10.

3.3.2.8 Short Rear, Full Forward Grain Configuration, SRFF

Heating rates were very low for this shot (30) and pressure rise was considerably delayed, so much so that only the beginning of the pressure trace was recorded.

3.3.2.9 Primer and Booster Only Configuration

A brief series of tests was conducted with both rear and forward grains inert in an attempt to assess the performance of the primer alone and the primer-booster combination. A pressure transducer was installed in the test fixture, but the level obtained during the tests was too low to record.

The primer alone caused the projectile to jump forward but the projectile retainer did not fail and it returned to its original position. This movement was signified by the impression left by the projectile nose on the clear plastic disc at the forward end of the round.

The addition of the booster did not cause the projectile retainer to fail during two tests and the projectile remained in its original position. The entire primer cup was consumed during both tests. Black powder gas flowed through this gaping hole, and around the exterior of the aft and forward grain. The entire aft end of the combustible case was consumed in addition to a section along the length of the case, extending almost the full length of the case, as shown in Figure 12. The plastic disc was blown out the front of the round, indicating that the gas escaped past the projectile and through the forward grain. The inert forward grain was clean and completely intact forward of the rotating band position which seems to indicate little flow through the grain.

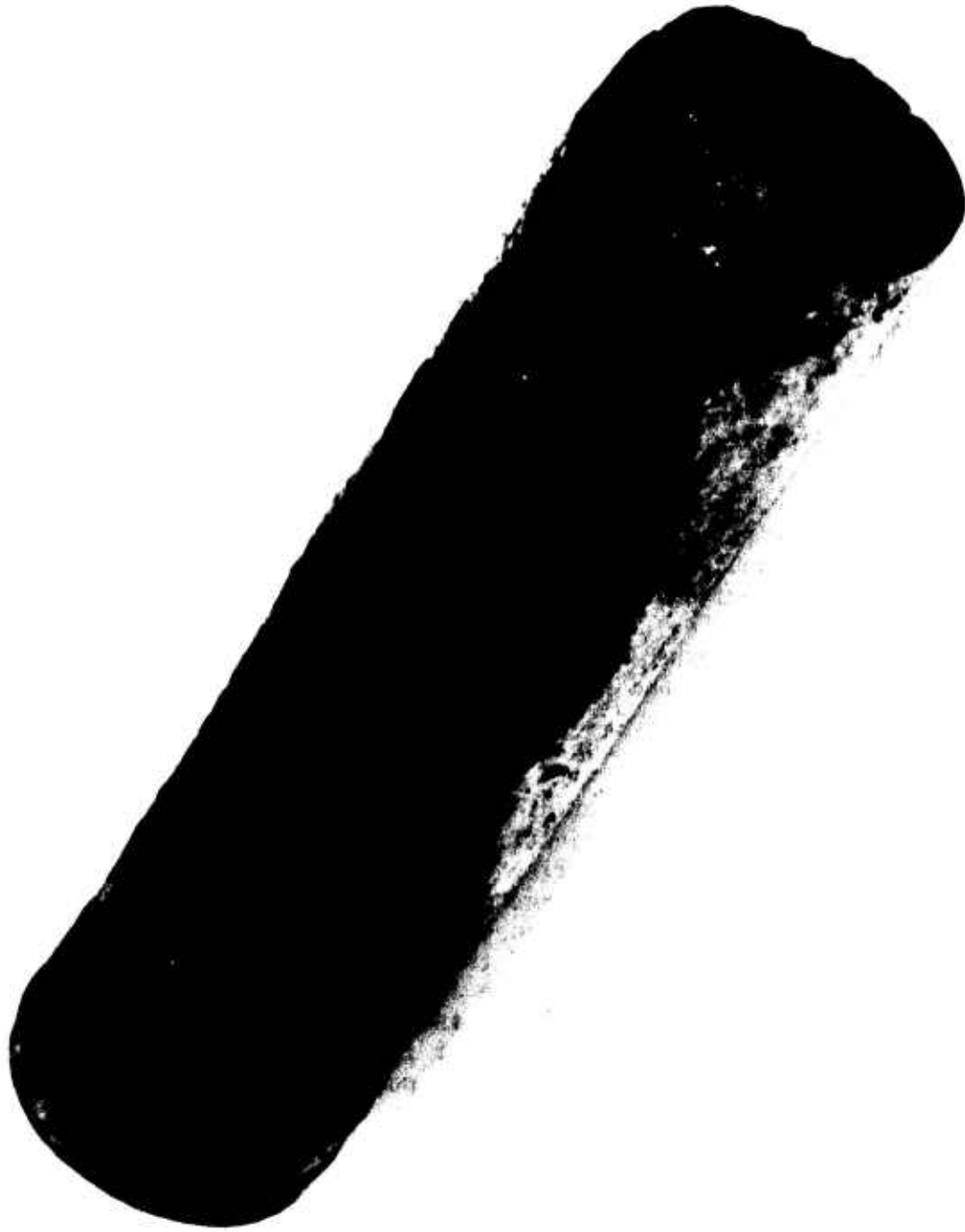


Figure 12. Illustration of the Unsymmetrical and Localized Heating Pattern Generated by the Booster with Inert Fore and Aft Grains

3.3.3 Summary of Significant Observations

This series of tests has yielded some very interesting and significant results. Attention is called to the most important results here and they will be included in the discussion in Section V, the critique of the GAU-7/A round.

1. The primer/booster combination does not always initiate projectile motion (3.3.2.9).
2. The black powder burns out the primer cup, the aft end of the combustible case, and flows over the exterior of the case and grain in an unsymmetrical manner (3.3.2.9).
3. Measured heat transfer supports the variability in heating at specific locations from test to test (3.3.2.1).
4. An observation was made that correlates intense heating at the forward end of the round with low peak pressure (3.3.2.2).
5. The greatest variation in performance was observed when the full aft grain was tested with an inert forward grain.
6. The GAU-7/A round performance is extremely sensitive to ignition, propellant mass, and other parameters:

<u>Test Number</u>	<u>Configuration</u>	<u>Propellant Weight (gm)</u>	<u>pmax (psi)</u>
32	MRFF	115.3	18,940
20, 26	FRMF	93.6	15,450
23	FRIF	33.6	13,500
9	FRFF	125.5	47,000

3.4 COMBUSTION STUDIES

One of the major tasks of this research program was to characterize the combustible components in a manner suitable for inclusion in the mathematical model. Combustion technology for both major components, the molded grain propellant and the black powder, is not well defined and much needs to be done in this area.

Two techniques were used during this program to characterize combustion of black powder and molded grain propellant. First, a closed cylindrical chamber was made to simulate one-dimensional ignition and combustion in a manner that could be duplicated by a one-dimensional code. In this way it was possible to use the mathematical simulation to help reduce and interpret the experimental results in a manner meaningful to the code. The second technique involved use of Calspan's Hi-Lo Bomb, a conventional closed bomb with a

high pressure igniter for rapid ignition. This provided molded grain combustion data that could be compared directly with its granular counterpart. The results from both experiments were then used in the simulation to verify the mathematical representation of molded grain combustion.

3.4.1 One-Dimensional Tests

The one-dimensional combustion tests were conducted in a steel chamber which could be divided into two chambers by a perforated steel plug. The object of the second chamber was to allow gas to flow through the molded grain during combustion, but this feature did not produce meaningful data and was not used during the primary tests. The chamber consists of a 4-inch long hollow cylinder with a 0.375-inch bore diameter and is closed at each end by steel blocks. The cylinder is clamped between them by 4 tie bolts. A fitting screws into one end block and it acts as a firing pin and primer holder. This end block also holds a pressure transducer as does the other block. The propellant slug was fitted snugly in the chamber and sealed to the chamber wall by epoxy cement. The free face of the cylindrical slug of propellant is exposed to the gases from the primer. Because of the long gap between the propellant and primer, a 6-grain booster charge of black powder was used to help ignite the propellant. It was held against the primer tube by a small paper diaphragm, cemented in place. Peak pressure and action time (time from primer strike to peak pressure) for a sampling of propellant tests, using propellant from the GAU-7/A rear grain, are shown in Table 6. Several attempts were made to correlate pressure rise data by using assumed burn rate functions in the mathematical simulations, but these were unsuccessful. The burn rate function and correlation with pressure rise data are shown in paragraph 3.4.3.

Black powder was also tested in the chamber in order to generate ignition and combustion rates as well as peak pressure information. The peak pressure and action time for a sampling of black powder tests are shown in Table 6. These data, the pressure time history, and other information found in the literature were used with the mathematical simulation to generate a consistent set of black powder combustion parameters.

Thermal conductivity of the virgin material, specific heat, and gas state constant are required model inputs. These parameters are not given in the literature, however, black powder consists mainly of potassium nitrate and the thermal properties of this compound ought to represent a reasonable first approximation. The International Critical Tables list 0.9 to 1.0 joules/gm°C as the specific heat and 300 to 600×10^{-4} watt/cm°C as the thermal conductivity for potassium nitrate. From these, the value of thermal conductivity in engineering units was taken to be 1.0×10^{-5} Btu/ft-sec-°R and the thermal diffusivity, 4.0×10^{-5} ft²/sec for use in the simulation. An approximate temperature of combusted black powder gas is given as 2200°C in Reference 2. This temperature, the black powder loading density, and peak pressure measured during black powder combustion experiments conducted during

TABLE 6. ONE-DIMENSIONAL CHAMBER TESTS

Charge Type	Weight (grains)	Length (in)	Primary Chamber Volume (in ³)	Peak Pressure (psi)	Time to Peak Pressure (msec)
Rear Grain	27.2	0.705	0.364	45,900	9.35
Rear Grain	27.2	0.704	0.364	44,280	8.20
Black Powder	25.0	--	0.389	9,600	17.00
Black Powder	50.0	--	0.336	22,100	9.00

this program were used to generate a state constant of

$$44 \frac{\text{ft-lbf}}{\text{lbm}^{\circ}\text{R}},$$

using the ideal gas equation of state. The density of black powder is approximately 1.86 gm/cc.

Black powder granules are irregular in shape and it is difficult to analytically describe the actual burning surface area. The approach was to represent the granules as small spheres in the mathematical simulation. The parameters of the burn function, $r = Bp^n$, were then adjusted until the pressure history generated by the computer simulation was reasonably close to that generated experimentally. In this way, the representation of black powder ignition and combustion in the model was slaved to the real world. In Figure 13, the experimental pressure curve is shown with the curve generated by the simulation with the revised thermal properties and the selected burn rate parameters $B = 0.0189$ and $n = 0.54$.

3.4.2 Closed Bomb Tests

Several closed bomb tests were conducted by burning portions of the rear and forward grains weighing approximately 30 grams each. This constituted 1/3 of the forward grain and 90 percent of the rear grain which was altered only by enlarging its I.D. to 0.6 inch to permit it to slide over the igniter of the bomb. The bomb used was a conventional 200-cc model that was provided with a Calspan-invented hi-lo igniter (Reference 3). This is a tube having closed ends, about 4 inches long, 1/2-inch O.D. and perforated with a number of small holes. The igniting powder, one gram of Dupont 700X powder for these tests, is burned inside the tube so that intensely hot gases are generated at a pressure far greater than that inside the bomb. This gas escapes in strong jets that serve to ignite the test propellant within the bomb.

Bomb pressure was recorded by oscilloscope and the pressure trace data (dp/dt versus p) was input to a digital computer program that solves the thermodynamic relation between mass rate of generation and rate of pressure rise, dp/dt , to determine the surface recession rate, i.e., the burn rate of the propellant and its corresponding burning surface area, given certain assumptions about propellant geometry during combustion. It was assumed in this case, that the geometry of the molded propellant after ignition was represented by a multitude of individual single-perf cylinders with initial dimensions of O.D. = 0.065 inch, I.D. = 0.008 inch and length = 0.085 inch (Reference 4). Results are shown by Figures 14 and 15 which also show the basic burn rate data of the propellant. The representation of the burning surface area of the molded propellant by the total surface area of individual elemental grains, in the same manner as granular propellant, is an extreme condition of the burning surface that results, as speculated by some people, if the molded grain shatters into bits immediately after ignition. This is fostered by a loosely bonded matrix which was observed in some aft grains.

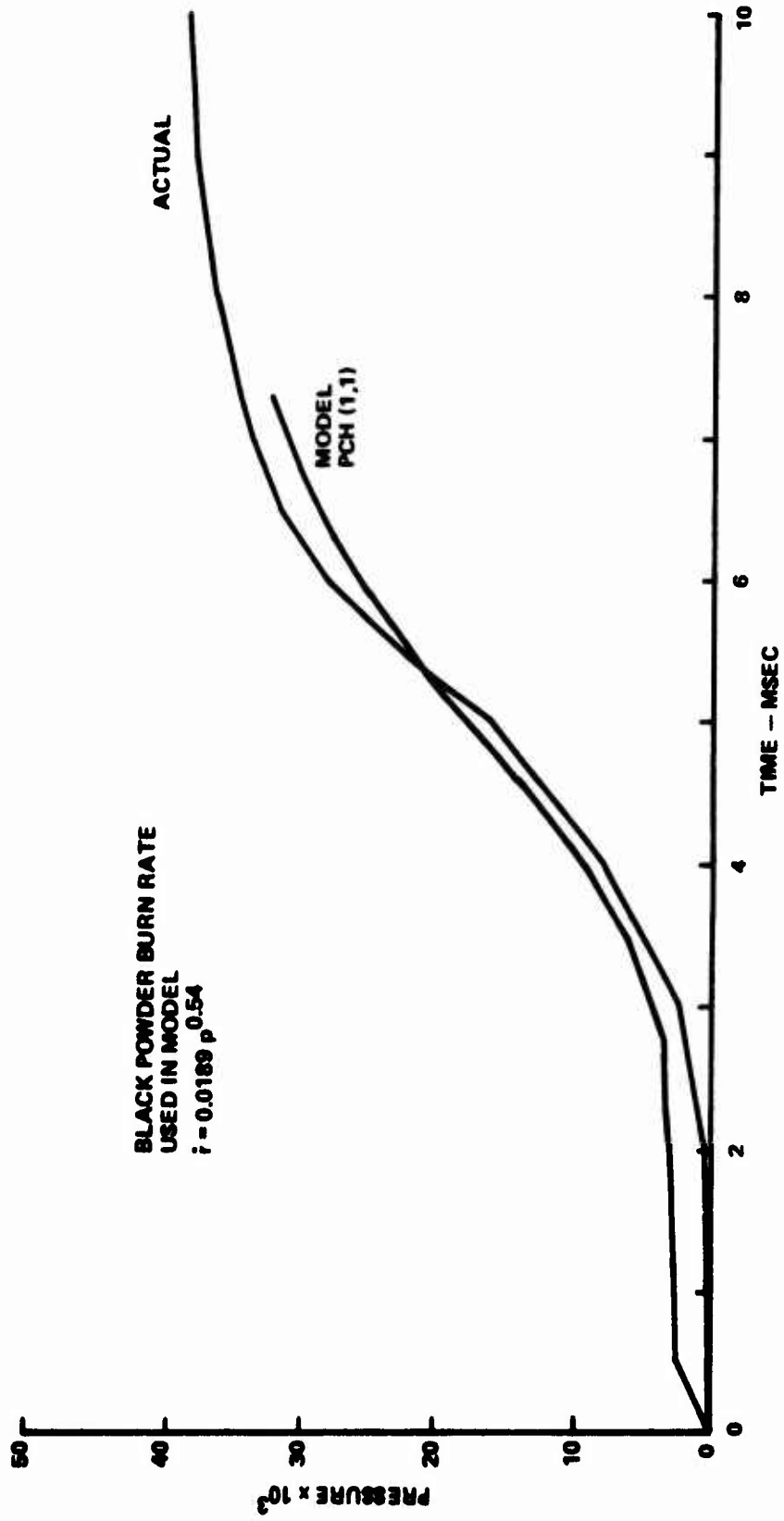


Figure 13. Comparison of Computed and Experimental Black Powder Combustion Results

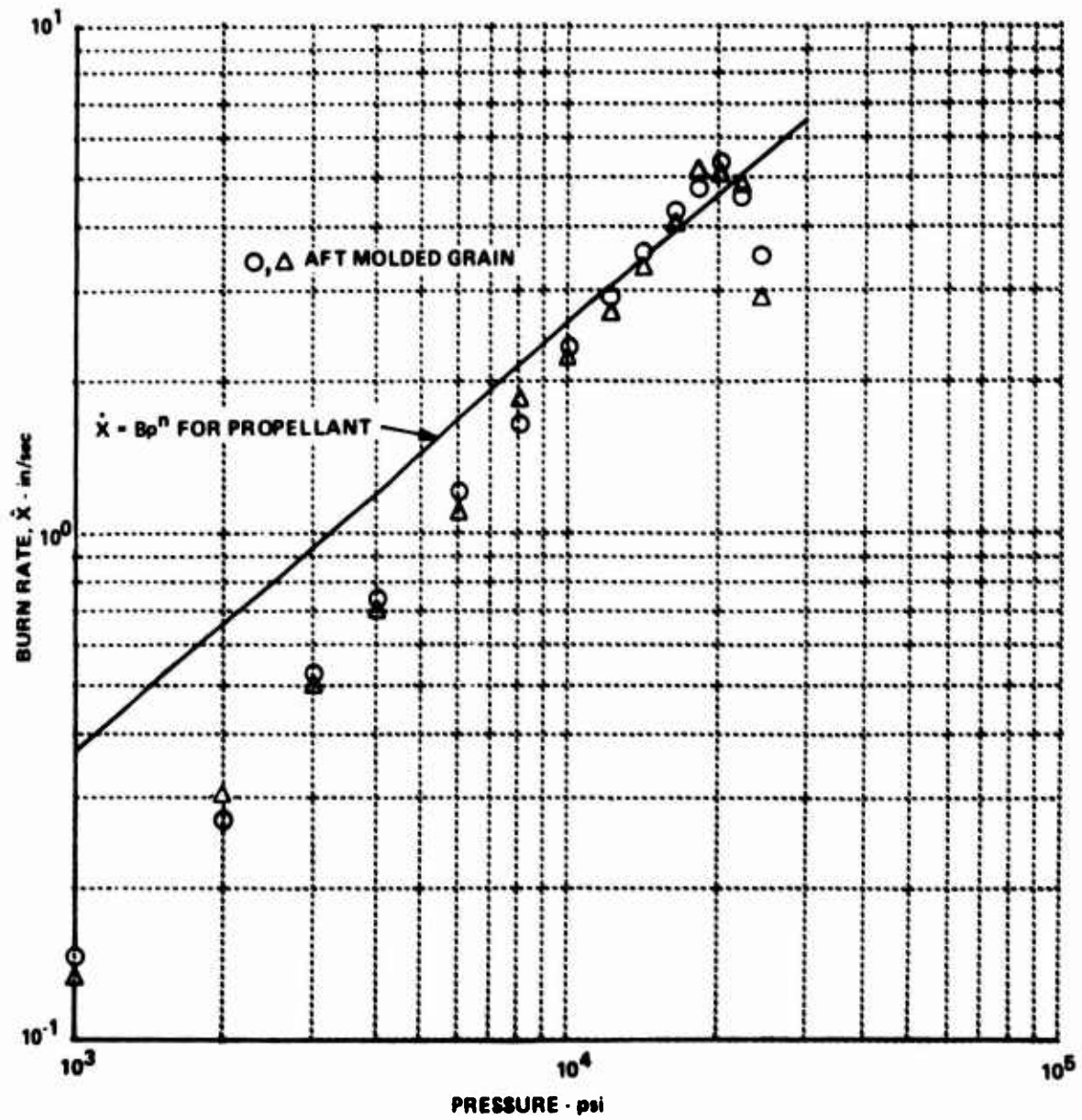


Figure 14. Closed Bomb Test Data - Aft Grain

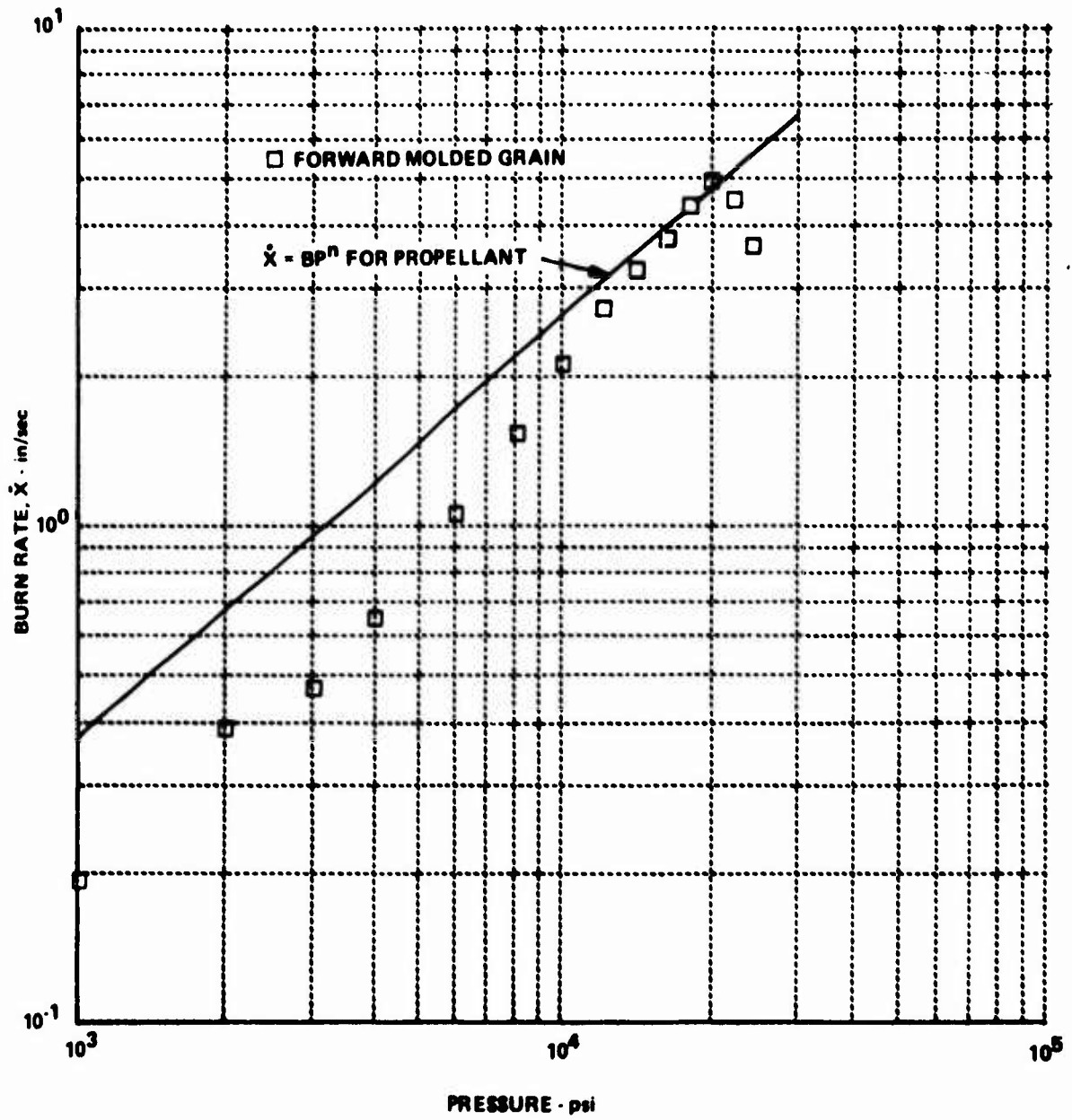


Figure 15. Closed Bomb Test Data - Forward Grain

3.4.3 Empirical Representations of Molded Grain Combustion

Combustion of molded grain propellant, unlike its granular counterpart does not have well defined burning boundaries or a geometric function that describes the shape change of the conglomerate. Grain breakup at various stages of the combustion cycle is a real consideration. Realistic and accurate representation of grain combustion is critical for the ultimate success of the mathematical simulation.

The problem at hand is to characterize the burning surface area of the propellant in a manner suitable for use in the computer code. This is discussed at some length in the Appendix. The burn rate is specified as

$$\dot{x} = \dot{x}(p) = Rp^n$$

The rate of gas generation is proportional to the product of burning surface area and the linear burn rate,

$$\dot{m}(t) = \dot{x}(p)A_b(t)$$

The closed bomb data reduction procedure assumed that $A_b(t)$ was the surface area form function for a granular bed, $A_{bmax}(t)$, so that

$$\dot{m}(t) = \dot{x}(p)A_{bmax}(t)$$

Use of this maximum surface area in the burn rate code generated a depressed value of computed burn rate, $\dot{x}(p)$, although the product of this depressed burn rate and $A_{bmax}(t)$ yields the true mass generation rate. The nominal burn rate, $\dot{x}_{max}(p)$, is assumed to be a known characteristic of the propellant. The actual burning surface area $A_b(t)$, can be determined by assuming that

$$\dot{m}(t) = \dot{x}(p)A_{bmax}(t) = \dot{x}_{max}(p)A_b(t)$$

The ratio of $A_b(t)/A_{bmax}(t)$ is plotted versus pressure in Figure 16 and fraction burned in Figure 17. This fraction burned is thought to be the most suitable parameter to correlate the burning surface area ratio because it relates the surface area to the propellant parameter rather than to the way it was burned. The burning area does not change suddenly or sporadically in a manner that might indicate sudden breakup of the molded grain. However, the ratio does approach and eventually exceed the granular bed value, as signified by $A_b(t)/A_{bmax}(t) > 1.0$.

As mentioned earlier, the Hi-Lo bomb employs a high-pressure igniter which minimizes ignition delay. However, this ignition time was not zero as was assumed in the data reduction procedure. Therefore, there is likely some effect of this delay on the results. The burning area reduction that appears near burnout may be partially a result of ignition delay where some sections of the grain burned out sooner than others.

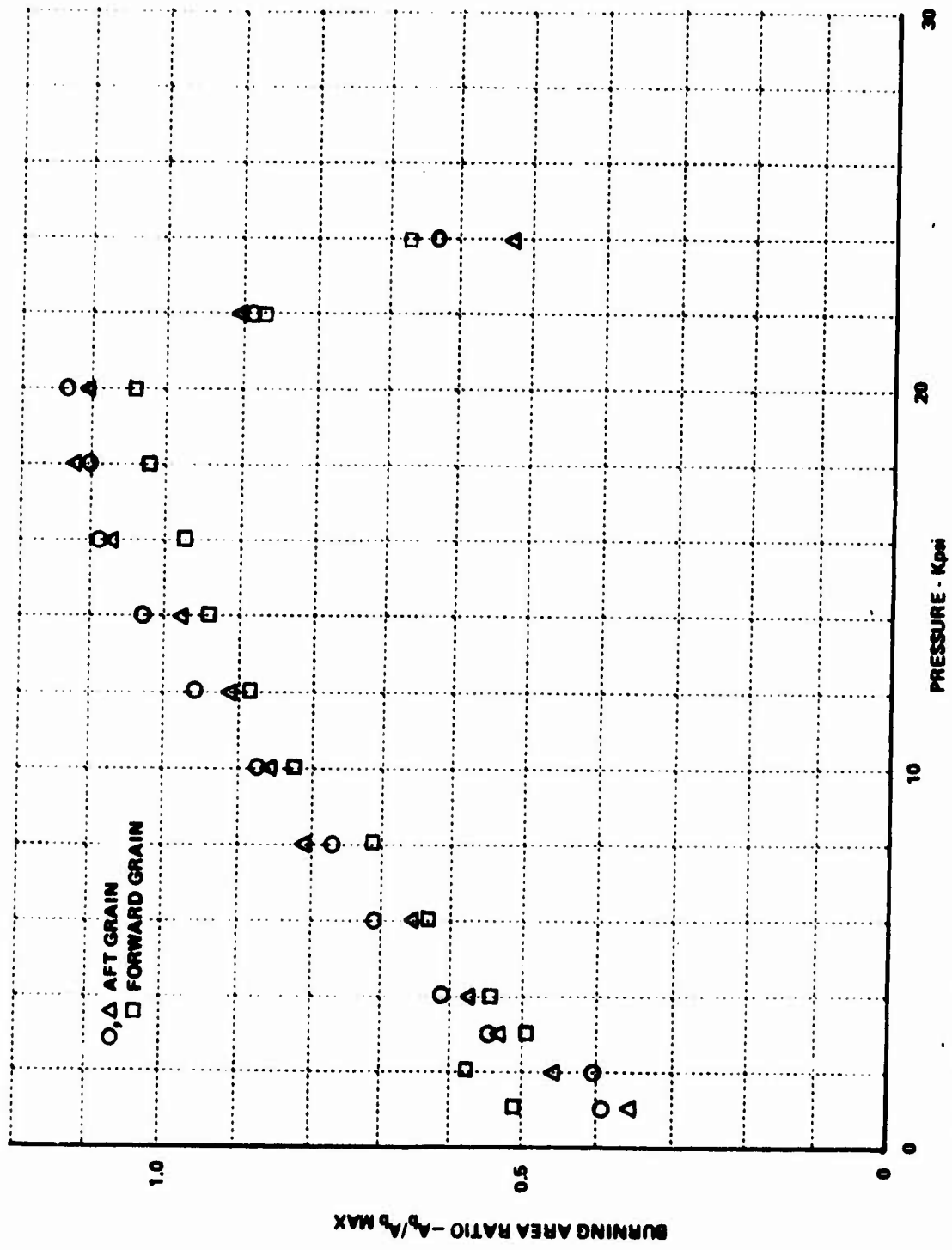


Figure 16. Burning Area Ratio Versus Chamber Pressure From 200-cc Powder Bomb Tests For Molded Propellant

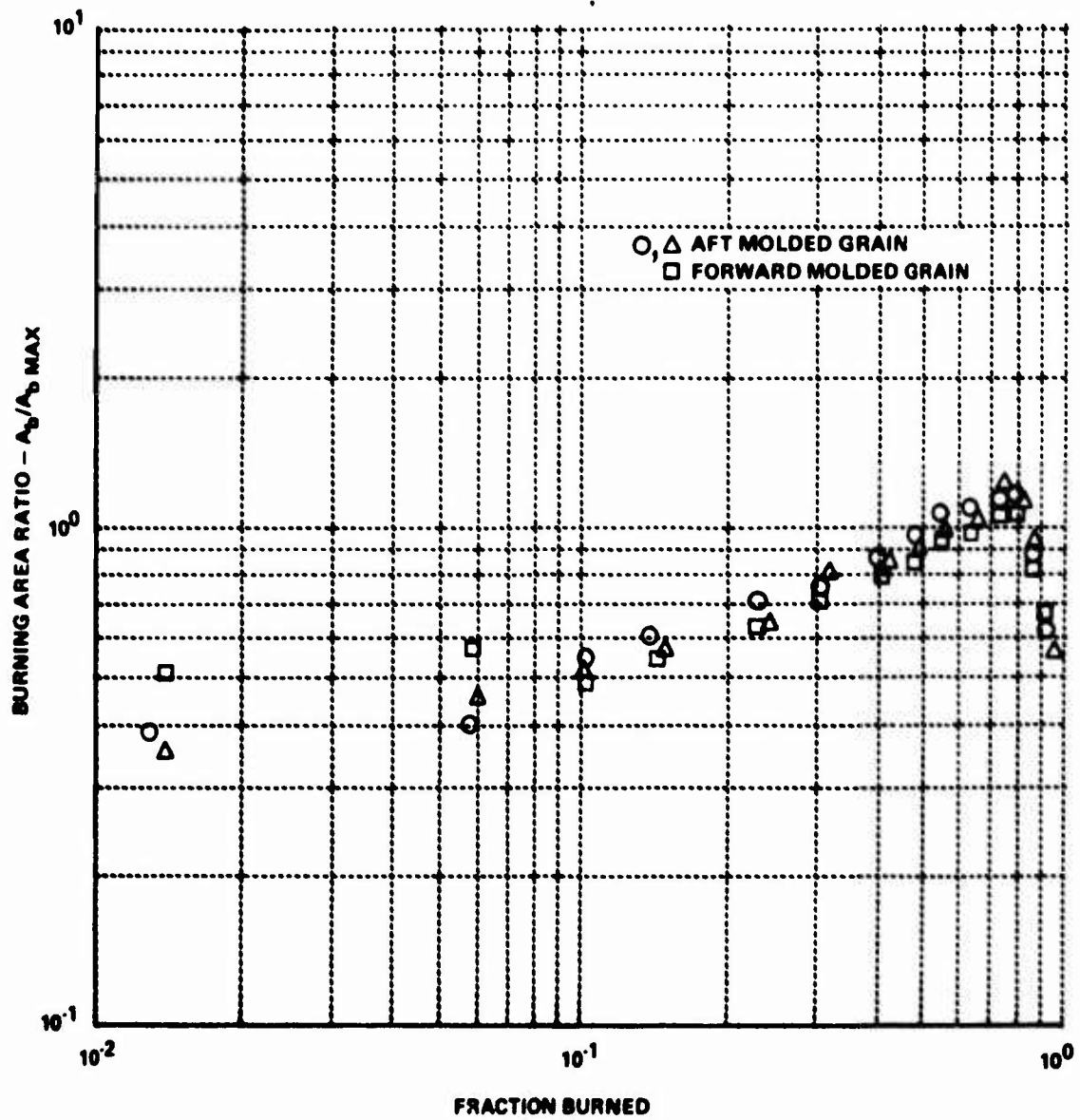


Figure 17. Correlation of Burning Surface Area with the Fraction Burned

A theory of molded grain combustion prior to breakup is formulated that seems to correlate these and other experimental observations obtained during the program. The theory simply states that the molded grain can be characterized as a solid chunk of propellant with uniformly dispersed voids of the same approximate size and number as the individual granules used to manufacture the molded grain.

The igniter gas flows into the void regions and ignites the exposed surfaces which are a composite of exposed granule surfaces and binder material. According to experimental observations, the total exposed initial surface area is roughly 35 percent of the area of a bed of loose grains with the same loading density. The flame spreads to the surface of adjoining void regions at a rate at least partially governed by the grain permeability. The surfaces surrounding the voids burn causing the void volume to increase in size. This has the effect of increasing the available burning surface area.

As combustion proceeds, adjacent void volumes begin to open into each other and coalesce. In addition, a phenomenon analogous to splintering of multiperf propellant occurs so that, near burnout, pieces of propellant break off and burn. This type of burning is regressive in that the total surface area decreases with time. Unusual grain breakup at granule boundaries may occur because the molded grain combustion rate reaches the rate of a bed of granules. However, this is an area that requires additional research. If the boundary between adjacent granules is well cemented, this boundary is as strong as the propellant granule itself and will not fracture easily. Therefore, it is believed that grain breakup will occur only at weak boundaries initially and thin surfaces as the voids increase in size and the breakup forces increase.

The representation of this theory in the model is purely empirical using burn rate data obtained previously with unmolded propellant and data obtained with Calspan's Hi-Lo Bomb. It is realized that this test device does not subject the grain to the high pressure and pressure gradient loads experienced in a gun. This deficiency is a topic for additional research. The expression for burn rate was assumed to be a function of the cumulative amount burned with the standard pressure dependency,

$$\dot{x} = f(F)Bp^n$$

where F is the fraction burned.

The quantity A_b/A_{bmax} , discussed earlier, represents the ratio of molded grain burning area to the burning area of a granular bed with the same amount of propellant burned. This area ratio was shown plotted against the fraction burned in Figure 17. The curve can be represented by the following equation:

$$A_b/A_{bmax} = \beta F^\eta$$

where $\beta = 1.10$ and $\eta = 0.37$ for $0 \leq F \leq 0.78$
and $\beta = 0.44$ and $\eta = -3.33$ for $0.78 < F \leq 1.00$

subject to the restriction that A_b/A_{bmax} not be less than some minimum value, say 0.35.

This burn rate expression was used with the one-dimensional version of the computer program to represent the one-dimensional transient combustion experiment reported in paragraph 3.4.1. The comparison of computed versus experimental pressure curves is shown in Figure 18. The time scale on the figure is that of the computed curve since the exact value of time zero is not known for the experimental curve. Agreement between the curves is excellent for pressures in excess of 15,000 psi. If the experimental curve were shifted to the right it would be observed that agreement is also excellent at pressures below 7500 psi. The slopes of the two curves differ between these two pressures for some unknown reason. However, we believe that this empirical representation of burning surface area together with the flame spread feature of the model represents a significant advance in representation of molded grain propellant combustion.

3.5 MISCELLANEOUS TESTS

3.5.1 Propellant Permeability

A simple apparatus was assembled for testing a sample slug of the propellant for permeability, or resistance to gas flow. The slug of propellant fitted snugly inside a hollow cylinder of 0.375 inch inside diameter against a small seat. It was sealed to the inside wall of the cylinder by epoxy cement so that no gas could bypass it. This device was connected to a cylinder of compressed nitrogen for providing a steady flow of gas. A sharp-edged orifice having a 0.064 inch throat diameter for choked flow was placed in the system downstream from the propellant for measurement of flow rate. Pressure gages were used to measure pressure upstream and downstream from the propellant samples. The nitrogen source was at room temperature so no other temperature measurement was required.

Repeated flow tests were conducted using a slug of propellant taken from the rear grain that was 0.375 inch long. Two source (upstream) pressures were used, 1940 psia and 5465 psia, and downstream pressures were measured at 118 psia and 256 psia respectively.

Flow rate was computed by the formula for choked flow using the flow coefficient data of Grace and Lapple (Reference 5). It was found to be 0.00712 lb/sec at the 1940 psia condition and 0.0153 lb/sec at the 5465 psia condition.

Resistance to flow was determined in terms of the parameter, $\phi_s D_p / f_m$, the quotient of shape factor divided by friction factor times particle size by means of a relation for computing pressure gradient through a bed of propellant grains. The relation is (Reference 6):

$$\frac{\phi_s^{3-n} D_p}{f_m} = \frac{4(1-\phi)^{3-n} L \rho V^2}{\phi^3 \Delta p 2g}$$

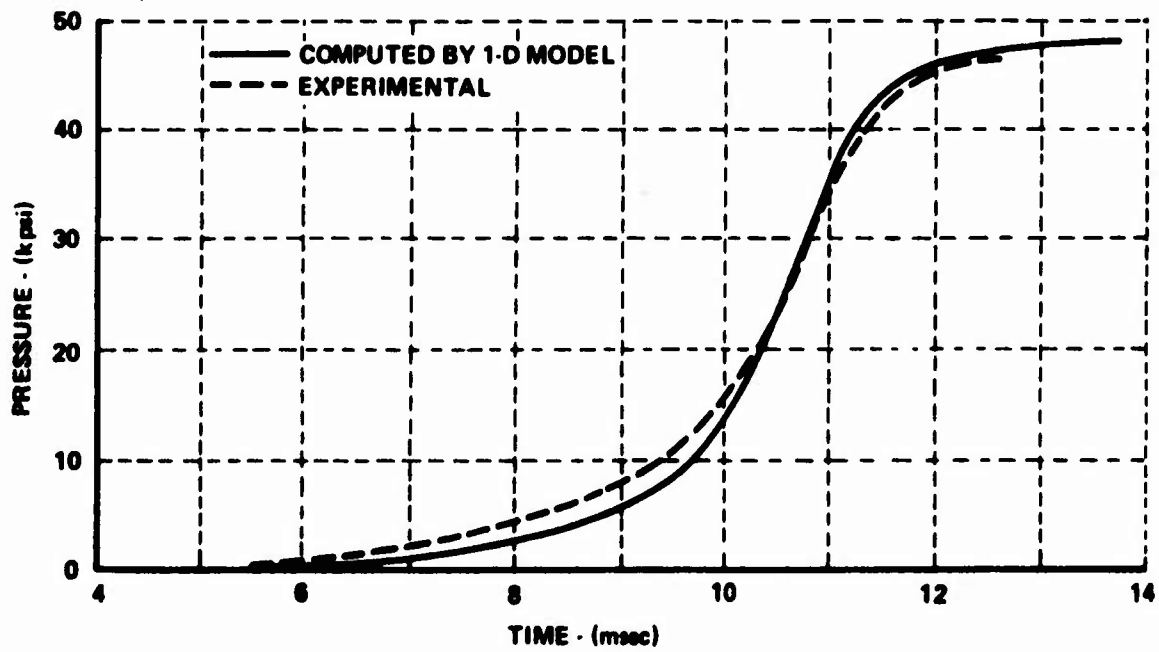


Figure 18. Comparison of Experimental Pressure Curve with a Computed Curve Using an Empirical Molded Grain Burn Rate Function

where g is acceleration of gravity
 L is bed length or distance along it
 n is Reynolds number dependent and is 2 for this work
 Δp is pressure drop along bed
 V is gas velocity that would prevail for an empty chamber
 ϕ is porosity (volume)
 ρ is gas density

The parameter

$$\frac{\phi S^D P}{f_m}$$

which is a permeability parameter, was found to be almost equal for the two test conditions, i.e.,

$$\frac{\phi S^D P}{f_m} = 13.9 \times 10^{-6} \text{ at } p = 1940 \text{ psia}$$

and

$$\frac{\phi S^D P}{f_m} = 15.2 \times 10^{-6} \text{ at } p = 5465 \text{ psia.}$$

3.5.2 Propellant Compressive Strength

Compressive strength tests were conducted on the rear charge propellant in an Instron Tensile Testing machine. Initial tests were conducted on cylindrical slugs that were machined from the rear charge to as large a diameter as practical and so that their end faces were flat to insure good results. The slugs were then stacked three high between the loading faces of the testing machine to minimize end effects.

The test slugs were 1.445 inches in diameter and 0.674 inch long and were concentric with the central hole of the rear charge. They crushed at a peak load of 1700 kg, which converts to a strength of 4400 psi in compression.

Additional compression tests were conducted with single slugs that were much smaller in diameter, 3/8 inch, after local weakness was discovered (during machining of the specimen grains for the closed chamber tests). When facing off the ends of some of these 3/8 diameter slugs the material was found to crumble even at very low tool feeds using speeds ideal for the normal material. In other words, the material had practically no tensile strength in small regions. Compression tests did not really reveal such extreme variability because it was impossible to machine a flat face on the weakest material. However, among the seven specimens compression tested, strength ranged from 5400 to 7500 psi.

The fracture surface of a typical crumbly region was examined by a scanning electron microscope at 133X magnification and compared with a fracture surface in strong material. The differences were extreme. The crumbly material surface was one that was textured by individual single grains and elements of binder material extending from scattered points that were apparently pulled like taffy when the material parted as shown in Figure 19. In addition, it was obvious that a relatively small proportion of the surface of individual grains had been covered with binder. Most of the space between grains was void space. By contrast, the fracture surface in strong material, Figure 20, showed that approximately half the individual grains were themselves fractured whereas none were seen in the weak material. Void spaces were rather widely scattered and there were separated binder elements.

These results indicate that the rear charge is not isotropic and the variation in properties increases as size of the specimen studied is decreased. Strength tests of specimens the size of the rear charge yield results that are not indicative of the variability, i.e., the inhomogenities in the material are quite localized.

3.5.3 Projectile Starting Force Tests

A force test was employed to determine the force characteristics of initial projectile movement through the forward charge, i.e., grain. Force was applied in an Instron model TTDM tensile testing machine, which was equipped with a force-time chart recorder. The first test was conducted on a round from which the rear grain and the cellulose shell had been removed. The round was placed between the loading faces of the machine in such a manner that load was applied to the projectile base and the reaction force was produced on the opposite end face of the forward grain. The projectile was forced to move at a steady speed of 0.5 cm/min relative to the forward grain. As movement proceeded, the load rose rapidly, at first. However, at 160 kg the rate of rise began to decrease until a peak of 222 kg was reached where the translation totaled 0.21 cm. By the time the projectile had travelled 0.4 cm the load had fallen to 30 kg. At this point the round was unloaded. Inspection revealed that the forward grain had failed, with a wide crack starting at the aft end and extending along the grain for 3.8 cm, where it turned circumferentially.

Further force testing was conducted with similar partial rounds placed within the chamber piece of the Eglin 25-mm firing fixture. In the next two tests the cellulose shell of the round was slipped over the forward grain and projectile assembly before inserting into the chamber for testing. However, these rounds were disassembled by slitting their shells (one slit was made lengthwise) and it was in this condition that the shell was used to confine the forward grain within the chamber.

During the first of these tests, the projectile was moved steadily within the forward grain. Load increased as for the previous test and at about 280 kg slope began to decrease until the load peaked at 320 kg and



Figure 19. SEM Photograph of a Molded Grain Exhibiting a Locally Weak Structure

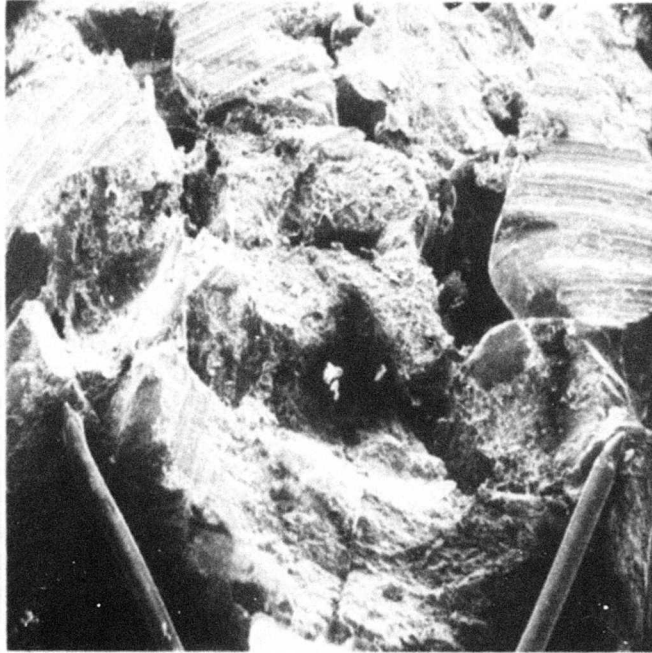


Figure 20. SEM Photograph of a Molded Grain Exhibiting a Strong Structure

travel was 0.267 cm. Loading was continued until the projectile had travelled 0.7 cm, whereupon it was unloaded. Again, a 3.8-cm-long crack was visible at the aft end of the forward grain. It was obvious that, even when confined within the chamber and its shell the forward grain was forced to spread as the base of the projectile carried its retainer into the bore of the grain.

A second partial round was force tested in the chamber piece but immediately upon detecting a drop in load the projectile was unloaded for inspection. Although this occurred at an unusually low load (133 kg), the procedure was consummated as planned and the round was removed from the chamber for inspection. No cracks were visible so it was loaded a second time. The load peaked at 195 kg and still no cracks were visible. A third loading was applied whereupon a peak of 188 kg was reached. This time a short crack was discerned, located about 1/4 inch around the perimeter from the slit in the shell. A final force test was made during which the projectile movement was continued for 0.5 cm after the peak load was reached (this time it was only 106 kg). Inspection revealed 4 distinct cracks separated by 1/2 inch or more around the periphery of the forward grain, none exceeding 1 inch length.

Four more rounds were partially disassembled for force testing within the chamber pieces, but without slitting the cellulose shell. Two were forced at a motion speed of 0.5 cm/min and two were forced at the much higher speed of 50 cm/min, in order to determine the effect, if any, of the speed of movement.

A peak force of 295 kg was reached during the first test of this group when the projectile had moved 0.217 cm. At this point force fell off to 125 kg and dropped gradually with distance moved until at 0.42 cm it was stopped. Force at this point was 25 kg. Visual inspection revealed several cracks, all shorter than 1 inch, at least 1/2 inch short of the leading edge of the rotating ring of the projectile as it was positioned within the forward grain.

The second test at 0.5 cm/min forcing speed, showed different results. Force peaked at 275 kg and 0.255 cm, dropped to 158 kg in a very short distance, rose to 166 kg, 0.033 cm further along, dropped slightly and then rose to 179 kg in 0.15 cm. As movement continued, force fell continuously until a plateau of 18 kg was reached and movement was stopped at 0.433 cm. Visual inspection revealed two cracks, one was 1 3/16 inches long and the other was 2 1/4 inch from the rear end of the grain so it extended well beyond the rotating band of the projectile.

Force tests at a speed of 50 cm/min showed a somewhat different force history. During the first test, the force rose rapidly to 258 kg and fell at about the same rate, i.e., 25,000 kg/min to a low point of 70 kg, rose to 165 kg at 1.716 cm and continually fell afterward until forcing was ceased at 100 kg and 2.383 cm. Visual inspection revealed a single crack 2.05 inches long which fell about 1/8 inch short of reaching to the position where the leading edge of the outer surface of the rotating ring stopped in the forward grain.

The force on second specimen increased at about the same rate as for the first test and peaked at almost the same force, 254 kg. It then fell off to a minimum of 125 kg and had risen erratically to about 200 kg when the test was stopped. Total travel of the projectile was 2.50 cm. Visual inspection revealed a single crack 1.95 inches long, considerably short of the leading edge of the rotating band, which stopped at 2.32 inches.

The results of the projectile forcing tests imply that lengthy cracks are produced in the forward grain as the projectile motion starts during firing. Furthermore, a sufficiently long crack may occur that provides a short circuit for chamber gases to bypass the projectile. This condition was not always obtained during the tests; in particular it was not obtained during the tests when the projectile was moved rapidly. However, the behavior of the rounds during these tests was not sufficiently different in any way to indicate that short circuiting could not occur during the rapid starts that prevail with firing.

SECTION IV
COMPUTER SIMULATION STUDIES

4.1 OBSERVATIONS

The TEAM code was developed during this program to provide an analytical tool to delve into the problems associated with molded grain, telescoped ammunition in general and the GAU-7/A round in particular. This particular ammunition has experienced excessive variability in the important performance criteria of action time, peak pressure, and muzzle velocity. This research program was established to gain insight into these problems so that the GAU-7/A ammunition might be redesigned with these problems eliminated.

The TEAM code was constructed to provide an analytical counterpart to diagnostic experimentation discussed in the previous section. The code was designed to evaluate the influence of certain ammunition parameters on overall ballistic performance. Variation in propellant combustion characteristics, in particular, is believed to be at least partly responsible for the observed ammunition variability. The code allows assumptions pertaining to ignition, burning surface area, basic burn rate, breakup and permeability to be evaluated. This, in combination with selected diagnostic experimentation, represents the approach used to isolate the sources of GAU-7/A variability.

The computer code contains many facets and possible avenues of calculation. The complexity of the simulation required that many assumptions and approximate empirical functions or techniques be incorporated to bridge certain gaps in the formal analysis. Extensive checkout of all the features of this complex code was not possible within the level of effort of this program. In addition, the formulation of the model did not address some items such as the grain breakup problem in a rigorous fashion, nor were such items as the combustible case and leaks around boundaries of the molded propellant grains treated. These and other phenomena ought to be included in the future to improve the overall predictability of the code. Nevertheless, the analytical technique has been established and the validity of its results has been partially verified.

The remainder of this section is devoted to discussion of code validation and sensitivity studies that have been conducted.

4.2 MODEL VALIDATION

The TEAM code is considered a deterministic model in that specific values must be assigned to each of the input parameters. Furthermore, specific coefficients must be assigned each of the empirical functions that

help comprise the model. The events that occur during an interior ballistic cycle are probabilistic in nature in that each input can be characterized by not one value but a distribution of values. It is customary to use the mean value of each parameter in the model and then vary them, one at a time, to determine the sensitivity of the parameters.

Unfortunately, many parameters are not well defined quantitatively. Molded propellant breakup and burning surface area in an actual gun environment must be assumed. Nominal values for linear burn rate and other propellant properties are available or can be calculated but their accuracy is uncertain. Other parameters such as heat transfer, the drag function, and barrel resistance are very approximate in nature, especially for molded propellant. The point to be made is that the TEAM code is input-limited in its predictive capability. Performance criteria of peak pressure and muzzle velocity can be met with a number of input combinations which makes code validation particularly difficult.

Fortunately, the TEAM code incorporated the techniques as well as actual subroutines of existing Calspan interior ballistic codes (Reference 1). The governing equations, their method of solution, and many of the peripheral calculations such as heat transfer, drag, projectile motion, and barrel boundary layer were all developed and used extensively on these other codes. These items were essentially validated when work on the TEAM code was initiated. Representation of molded grain and black powder combustion were validated through favorable comparison of the computed and measured pressure histories shown in paragraph 3.4.

The GAU-7/A ammunition exhibits a wide variation in performance with no change in ammunition parameters. For specific inputs to the TEAM code, it is not known what the computed result should be within acceptable limits. Therefore, the main criterion adopted as a basis for validation is that the computed performance histories should show some of the characteristics of the experimental results.

The combustible case was not included in the mathematical model of the GAU-7/A ammunition. The inability to represent case combustion effects and the volume occupied by the case is expected to introduce inaccuracies into the calculated results. Some data were obtained from GAU-7/A ammunition fired in a steel case, which is a configuration that more nearly matches the code formulation. The important code inputs for this configuration are given in Table 7.

The plotted pressure-time history using a standard projectile is compared with a measured curve using a 2300-grain projectile in Figure 21. The computer-generated curve contains certain assumptions that are indicated on the figure. The TEAM code does not calculate molded grain breakup, so assumptions must be made as to time and nature of the breakup.

TABLE 7. TEAM CODE INPUTS FOR VALIDATION CALCULATION

Propellant properties: Burn rate function: $\dot{x} = (0.001074p^{0.848})(1.096F^{0.369})$

where \dot{x} is burn rate - in/sec

p is pressure - psi

F is fraction burned

Propellant density - 104.2 lbm/ft³

Molded grain density - 87.26 lbm/ft³

Energy - 1300 Btu/lbm

Granule inner diameter - 0.008 in

Granule outer diameter - 0.065 in

Granule length diameter - 0.085 in

Permeability ($\frac{\phi_S D}{f}$) - 15×10^{-6} ft

ϕ_S is shape factor

D is effective diameter

f is fraction factor

Physical Characteristics: Aft grain weight - 0.085 lbm

Aft grain length - 1.10 in

Aft grain outer diameter - 1.485 in

Aft grain inner diameter - 0.330 in

FWD grain weight - 0.200 lbm

FWD grain length - 4.673 in

FWD grain outer diameter - 1.485 in

FWD grain inner diameter - 0.984 in

Chamber diameter - 1.485 in

Projectile and Barrel Properties: Projectile weight - 0.4286 lbm

Projectile moment of inertia - 0.167×10^{-4}

Barrel length - 84 in

Retainer failure strength (shot start) - 750 psi

Rotating band engraving force - 2000 psi

PRES: 10,000 psi/div
TIME: 2.0 msec/div

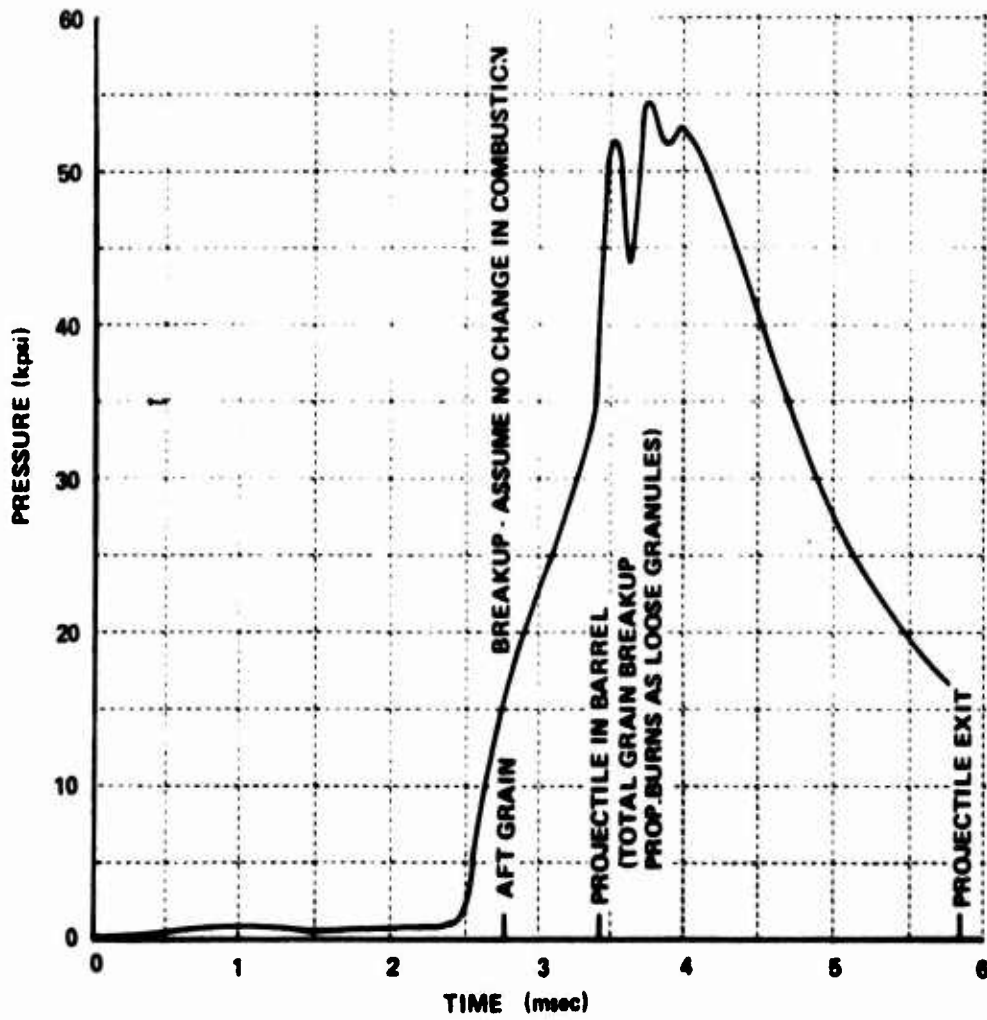
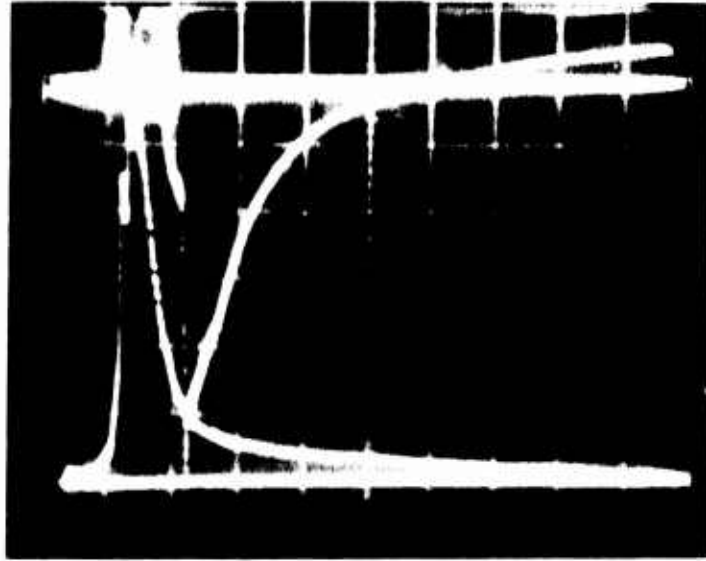


Figure 21. Comparison of Measured and Computed Pressure Histories Using the Inputs of Table 7

The code begins the calculation with the aft grain represented by an axisymmetric formulation. This involves many calculations and it is desirable for the sake of economy to convert the axisymmetric formulation into a one-dimensional formulation at the earliest possible time. This was chosen to occur at the time the entire aft grain was ignited and the projectile was undergoing significant movement. The change to a one-dimensional formulation involved redistributing the propellant as if it were broken into large pieces. The burn rate of the propellant was assumed to be unaffected by this action. Later, after the projectile entered the barrel, the three parallel grid networks of the forward grain were converted into a single one-dimensional matrix and merged with that of the aft grain. After this breakup, all propellant was assumed to be in the form of loose grains and burn accordingly.

The computer-generated chamber pressure history in Figure 21 exhibits some interesting dynamics in the region of peak pressure that are quite similar to those observed experimentally during some tests. These dynamics are largely driven by breakup-related phenomena. The rise portion of the history is accurate initially but lags before finally exhibiting a rapid rise to peak pressure. This indicates that the propellant burn rate used in the code was too low during the depressed region but that, elsewhere, representation was adequate. After peak pressure, the computed and measured data were alike.

The computed muzzle velocity for the run discussed in the preceding paragraph was 3926 ft/sec while the actual velocity of a steel cased round is about 3650 ft/sec. A second run was made with the energy content of the propellant reduced to 1000 Btu/lbm. This run generated a peak pressure of 73,000 psi and a muzzle velocity of 3700 ft/sec. The measured and computer-generated pressure curves, including dynamics, are quite similar as shown in Figure 22.

Therefore, the computer code has demonstrated the ability to generate unique features in pressure curves which is indicative of accurate representation of fundamental physical phenomena. At this time, many of the fine points and subtleties are not sufficiently well formulated for the code to be truly predictive. However, it has been demonstrated to be a valuable tool to help understand experimental results.

4.3 PARAMETER SENSITIVITY STUDY

A parameter sensitivity study was run using the TEAM code to assess the importance of various ammunition physical and phenomenological characteristics. The results of this study are shown in Table 8. The more significant code inputs for the base run are given in Table 7. Each run in the study incorporated the inputs or assumptions of the base run except for the single change as noted.

PRES: 10,000 psi.
TIME: 2 msec/div

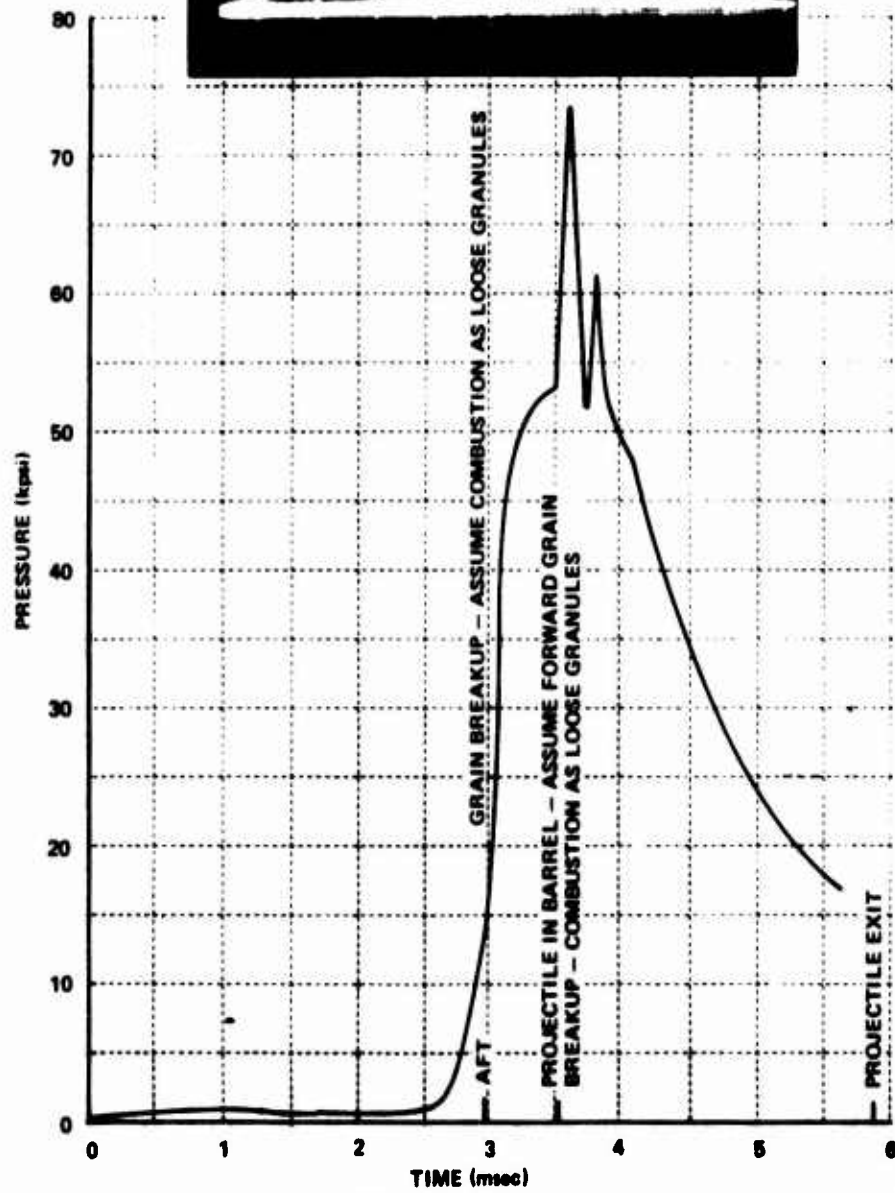
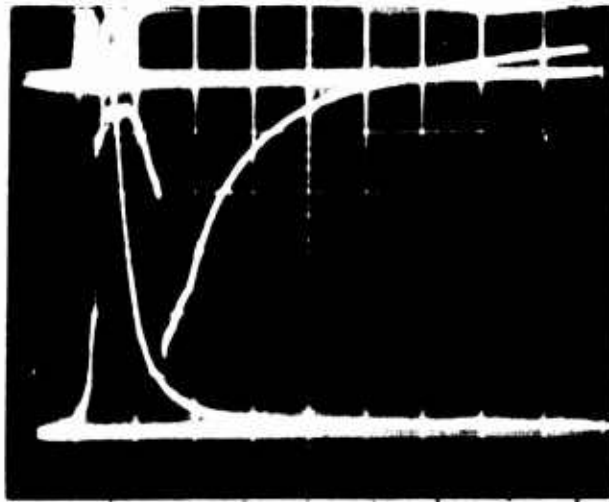


Figure 22. Comparison of Measured and Computed Pressure Histories

TABLE 8. GAU-7/A PARAMETER SENSITIVITY STUDY

	Grain Breakup Mode ^a	pmax-psi	mv-ft/sec	Act. time msec	Unburned Prop. lbm
Base Run (see Table 7)	1	42,600	3640	5.99	0.93×10^{-2}
Perforation Diameter = 0.007 (-0.001 in)	1	41,000	3607	6.03	0.11×10^{-1}
Outer Diameter = 0.060 (-0.005 in)	1	52,000	3841	5.80	0.16×10^{-2}
Shot Start = 2500 psi (-500)	1	42,000	3646	6.49	0.86×10^{-2}
Engraving Force = 5000 psi (+3000)	1	43,000	3645	6.00	0.91×10^{-2}
Velocity Related Resistance Function	1	42,600	3646	6.01	0.93×10^{-2}
Propellant Chemical Energy - 1400 Btu/lbm (+100)	1	46,000	3761	5.85	0.63×10^{-2}
Burn Rate Coeff. = $0.001274 (+18.6\%)$	1	70,000	4053	5.39	0.16×10^{-2}
Perm. factor = $15 \times 10^{-5} (x10)$	1	38,100	3601	5.41	0.72×10^{-2}
No leakage past projectile	1	70,000	3916	5.59	0.32×10^{-2}
No. Prop. Ignition Ahead of Projectile	1	33,700	3492	6.23	0.16×10^{-1}
Base Run with Breakup	2	>100,000	4270	4.39	0.16×10^{-2}
Base Run with Breakup	3	80,000	4049	4.64	0.16×10^{-2}
Base Run with Breakup	4	55,000	3926	5.85	0.81×10^{-3}
Comb. Case (Chamber dia. = 1.685 in)	1	23,500	3121	9.83	0.16×10^{-2}
Comb. Case (Chamber dia. = 1.685 in)	4	39,600	3593	7.82	0.98×10^{-3}

- a) Grain Breakup Mode
1. Aft grain breakup assumed to occur shortly after ignition and forward grain breakup occurs after projectile is seated in barrel. Assumed to change permeability to value of a loose granular bed but not to influence burn rate.
 2. Same as 1 except burn rate is always granular bed value.
 3. Same as 1 and 2 except forward grain burn rate changes to granular bed value after breakup.
 4. Same as 1 and 3 except that aft grain burn rate changes to granular bed value after projectile reaches barrel.

4.3.1 Physical Properties

These properties include dimensional and chemical characteristics of the propellant granules that comprise the molded grain. Also included here are items such as grain permeability and burn rate. The outer and perforation diameters of the propellant granules alter the burning surface area and small changes in those parameters have a relatively large effect on ammunition performance. Propellant energy content and burn rate both serve to increase peak pressure and muzzle velocity. The percentage of increase in peak pressure is roughly the square of the change in muzzle velocity. The grain permeability, on the other hand, lowers peak pressure with little change in muzzle velocity. Apparently, low permeability prevents gas from leaving the molded grain during combustion. This causes an elevated internal pressure, and, assuming that the pressure-dominated burn rate law holds, the combustion rate is increased, resulting in an increased peak pressure. These factors are important in the design of high velocity rounds.

4.3.2 Phenomenological Properties

These are defined to include shot start and projectile resistance forces, gas flow into the barrel ahead of the projectile and ignition phenomena. Forces tending to retard the projectile do not appear to have a significant impact on peak pressure or muzzle velocity. Shot start pressure has to be relatively low, below the compressive strength of the forward grain. Pressure rise rates are rapid and the small possible variation in shot start is swamped by the massive gas generation of the aft molded grain. By the time the projectile reaches the barrel, the computer solutions indicate the velocity is in the vicinity of 1000 ft/sec and its momentum is sufficient to overwhelm the plastic rotating band engraving force.

The item identified as velocity-related resistance function is an attempt to account for back pressure due to compression of gas in the barrel ahead of the projectile. The code assumes that this gas is ambient air initially in the barrel. It does not include combustion gas introduced ahead of the projectile. This is judged to be a deficiency that ought to be upgraded. The resistance function did not make a significant change in muzzle velocity, although inclusion of gas leakage might.

Gas leakage ahead of the projectile was found to be an important parameter. The amount is small, 0.0015 lbm for a typical run. This amounts to about 0.5 percent of the total charge weight. However, it represents a much higher percentage of the gas in the system at the time the leakage occurs, which is prior to the time the projectile enters the barrel. If this leakage is prevented, the pressure boot-strap effect is observed whereby, not only is pressure increased due to an increased amount of gas but the increased pressure increases the rate of gas generation. Therefore, peak pressure is increased substantially.

The TEAM code indicates that ignition is usually complete before the projectile enters the barrel. If ignition at a point on forward grain is allowed to proceed only after the projectile has passed that point, the computed peak pressure and muzzle velocity are greatly reduced. Action time and the amount of unburned propellant at the end of the ballistic cycle are also high. The effects of this slight delay in surface ignition are probably amplified by the pressure-boot-strap effect working in conjunction with projectile motion.

4.3.3 Grain Breakup

Propellant grain breakup has been found to be the single most significant factor in performance of GAU-7/A ammunition. The TEAM code, as mentioned in 4.2, reduces the complexity of computation after the aft grain is ignited and after the projectile enters the barrel. This collapse from axisymmetric and multiple one-dimensional grid matrices to a single one-dimensional matrix was done for the sake of economy but there is also physical significance to these events. As long as the projectile is stationary, gas generated within the aft grain flows into a small volume occupied by the booster. Pressure gradients and forces tending to break the grain are relatively small. When the projectile begins to move, the volume increases dramatically, and more gas must flow from the grain to fill the volume. Pressure gradients within the aft grain, governed by the permeability, become large. This is the condition required for grain breakup. A similar event happens to the forward grain when the rapidly accelerating projectile enters the barrel.

Thus, the collapse to a one-dimensional matrix represents grain breakup. However, the TEAM code currently bases this solely on projectile position rather than pressure gradient and grain strength, so while breakup is a real phenomenon, the actual time and degree of breakup are uncertain. Experience with the code seems to indicate that the molded grain breaks up into the granule elements that it was made from and burns accordingly. For now, these assumptions regarding burning surface area must be made in accordance with the code matrix conversion.

4.3.4 Combustible Cased Ammunition

The TEAM code does not address ignition or combustion of the combustible case. It has been treated as just an empty void, which is the situation for the data shown in Table 8. This gives the correct chamber volume after the case is consumed but depresses the performance due to loss of case combustion products and excessive initial volume. Therefore, the TEAM code is better suited for metal cased ammunition although it would increase the versatility of the code to include this feature.

SECTION V

CRITIQUE OF GAU-7/A AMMUNITION

The firing sequence of GAU-7/A ammunition was given in Section II as it was envisioned during formulation of the mathematical model. The experimental and computer simulation efforts described in Sections III and IV have shed much light on the potential sources of variability in GAU-7/A ammunition performance. The firing sequence will be repeated with special emphasis pertaining to sources of variability.

The firing sequence is initiated when the primer is fired. Tests indicated that the GAU-7/A primer may be sensitive to strike force, as well as moisture, providing a source of variability early in the firing cycle. The primer output ignites the black powder booster. In theory the booster charge is supposed to initiate projectile motion by creating a pressure at the projectile base high enough to cause the retainer to fail. In practice, this was not observed during the two instances the fore and aft grains were inert. Therefore, it can be stated that the booster does not always initiate projectile motion.

A plastic sleeve separates the booster from the inner surface of the aft grain to provide an ignition delay of that surface until projectile motion has created free volume. However, since the booster does not always initiate motion, combustion of the aft grain is necessary to initiate projectile motion. The booster gas burns out the primer cup, flows out the aft end and over the exterior surface of the round in an unsymmetrical manner (see Figure 12). In addition, gas flows through imperfections in the glue joint that bonds the aft grain and projectile retainer. This gas flow over and around the aft and forward grain follows a somewhat random path that introduces variability in ignition of the fore and aft grains as well as the combustible case. Heat transfer data measured at the forward end of the round during tests with inert components varied substantially from test to test in support of this contention. During these tests it was observed that high heat transfer at the forward end was indicative of a low pressure run. Perhaps this indicates a higher loss of gas into the barrel ahead of the projectile, yet another potential source of variability.

Once the retainer fails, the projectile experiences practically no resistance until it enters the barrel. Both grains become completely ignited during this period, the aft grain somewhat earlier than forward grain. It is during this period that grain breakup is extremely important. The marked similarity between experimental and simulation results when grain breakup assumptions were incorporated into the simulation is strong evidence of the breakup influence on performance levels. It

is surmised that projectile motion causes the free volume to expand which in turn causes increased gas flow from the grains into the void volume. Large pressure gradients are established in the aft grain first, and then in the forward grain, that eventually cause the grains to break up. Therefore, the aft grain is believed to fail before the projectile enters the barrel, and the forward grain just after.

Breakup causes a large increase in the permeability of the bed and the gas generation rate. By trying different assumptions in the TEAM code as to the degree of breakup, the best agreement with experimental results is obtained if it is assumed that the propellant breaks up into the granules used to make the molded grain. However, it has been observed that some boundaries are as strong as the material itself while others are very weak. The weak boundaries will obviously fail but the strong boundaries may not. Therefore, the extreme variability in structural integrity that was observed in the aft grain is believed to be a source of GAU-7/A variability.

The forward grain did not appear to exhibit the extreme variation in performance although it was not studied as extensively as the aft grain. Projectile velocity and pressures are high when it fails so failure is bound to be more rapid and complete. This is contrasted with the relatively long heatup and low pressure combustion period experienced by the aft grain where pressures are the same order of magnitude as the material strength. Breakup in this case will not be as decisive or complete.

Computer simulations indicate the projectile velocity is quite high when it reaches the barrel. The high projectile momentum drastically reduces the effect of engraving force on round performance.

The information amassed during this program indicates that the following conclusions can be drawn:

1. A source of GAU-7/A ammunition action time and performance variability is due to variation in interaction between the primer/booster products and the other components, as well as variation in the combustion process.
2. The similarity between experimental results and analytical results involving breakup assumptions indicates the strong influence of grain breakup on performance levels.
3. The variability in structural integrity of the aft grain, the importance of grain breakup, combined with large variability in aft grain performance when tested alone indicate it is a significant contributor to GAU-7/A variability.

4. The large contribution of the combustible case to muzzle velocity, a result of both its combustion products and its gradual creation of free chamber volume as a result of combustion, combined with its ability to absorb moisture make it a strong potential contributor to performance variability.
5. The forward grain has not been adequately assessed but appears to be more consistent than the aft grain.

Recommendations for improved ammunition, based on these conclusions, include as a minimum:

1. Design consistent primer/booster.
2. Improve quality control of molded grain components.
3. Eliminate or improve combustible case.
4. Give positive direction to booster products of combustion.

REFERENCES

1. Fisher, E.B., "Propellant Ignition and Combustion in the 105mm Howitzer," Calspan Report No. VQ-5524-D-1, January 1975.
2. Chemistry and Technology of Explosives, Urbanski, Vol. 3, Pergamon Press, 1967.
3. Fisher, E.B., and Trippe, A.P., "The Hi-Lo Bomb--A New Device to Evaluate Propellant Combustion Properties," Calspan Internal Research Report; Project No. 85-677, March 1975.
4. Personal communications with O. Heiney, AFATL, Eglin AFB, March 1976.
5. Grace, H.P., and Lapple, C.E., "Discharge Coefficients of Small Diameter Orifices and Flow Nozzles," Trans. of the ASME, July 1951.
6. Perry's Chemical Engineer's Handbook, Fifth Edition, pg. 5-52, 5-53, McGraw-Hill, 1973.

APPENDIX

MOLDED GRAIN PROPELLANT POROSITY AND EXPOSED SURFACE AREA

An important parameter in propellant combustion is the exposed surface area, or the area that is free to burn. For loosely packed granular beds, this quantity can be determined in terms of individual grain dimensions and the total number of grains. The latter quantity is expressed in terms of porosity, the void volume fraction. The following items are defined for GAU-7/A propellant:

$$\begin{aligned} \rho_g &= \text{propellant density} = 0.0603 \text{ lbm/in}^3 \\ \rho_b &= \text{bed or molded grain density} = 0.0505 \text{ lbm/in}^3 \\ \phi &= \text{porosity of void fraction defined so that } \phi = 1 \text{ is all gas} \\ &\quad \text{and } \phi = 0 \text{ is all solid} \\ V_b &= \text{bed volume} \\ V_g &= \text{grain volume} = (1 - \phi)V_b \\ \phi &= 1 - \frac{\rho_b V_b}{\rho_g V_b} = 0.1625 \end{aligned}$$

$D, d, L =$ individual grain outer diameter, inner diameter and length = 0.065, 0.008, and 0.085 in, respectively.

The volume of an individual single-perf grain is given in terms of dimension and the porosity as:

$$V_g = \frac{\pi}{4} L (D^2 - d^2)$$

and the number of grains per unit volume is:

$$\begin{aligned} N &= \rho_b / \rho_g V_g = \rho_b / \frac{\pi}{4} \rho_g L (D^2 - d^2) \\ &= (1 - \phi) / \frac{\pi}{4} L (D^2 - d^2) \end{aligned}$$

The surface area per grain is:

$$S_g = 2 \left[\frac{\pi}{4} (D^2 - d^2) \right] + \pi L (D + d)$$

The total surface area per unit volume of granular bed is then:

$$S_b = NS_g = (1 - \phi) \left[\frac{2}{L} + \frac{4}{D-d} \right] = 78.5 \text{ in}^2/\text{in}^3$$

This is the maximum burning surface area/unit volume of propellant. Assuming the volume is occupied with whole grains, all surface area of the original elements is exposed and subject to heating and combustion.

Thus, as $\phi \rightarrow 0$ (all solid), $S_b \rightarrow \frac{2}{L} + \frac{4}{D-d}$

However, the element boundaries in a molded grain are not all free. Solvent applied to the elements tends to make adjacent element boundaries coalesce and become nonexistent. In this case as $\phi \rightarrow 0$, $S_b \rightarrow 0$. The molded grain porosity consists of the perforation volume and the voids dispersed throughout the molded grain as a result of the random packing of cylindrical shapes. Neglecting the ends of the perforations, which may be closed as a result of the solvent/compressing operation, the surface area/unit volume within the perforations is

$$S_{bp} = \frac{4(1-\phi)d}{D^2 - d^2}$$

The volume contained within the perforations is:

$$\phi_p = \frac{(1-\phi)d^2}{D^2 - d^2}$$

Total, intergranular volume excluding grain perforations is:

$$\phi_I = \phi - \phi_p = \frac{\phi D^2 - d^2}{D^2 - d^2}$$

With quantities given earlier for GAU-7/A ammunition, the intergranular porosity is 0.150.

If the number of voids can be assumed to be equal to the number of grains, then the volume per void is:

$$\phi_V = \phi_I / N = \frac{\pi}{4} L (\phi D^2 - d^2) / (1 - \phi)$$

Characteristic void radius:

$$r = \left(\frac{3\phi_V}{4\pi} \right)^{1/3}$$

Surface Area/Void:

$$S_V = 4\pi \left[\frac{3}{16} L \frac{\phi D^2 - d^2}{1 - \phi} \right]^{2/3}$$

Surface Area/Volume:

$$S_b = \frac{1}{D^2 - d^2} [3(\phi D^2 - d^2)]^{2/3} \left[\frac{16(1-\phi)}{L} \right]^{1/3} = S_V \cdot N$$

With these assumptions and the dimensions given earlier, the characteristic void diameter is 0.045 inch and the surface area per unit volume is $19.6 \text{ in}^2/\text{in}^3$ excluding the area contained in the perforations. If this perforation area is included, the surface area is increased to $26 \text{ in}^2/\text{in}^3$. From observation, the actual void dimension may be somewhat smaller. If 0.02 inch is a representative diameter of a spherical void, then the spherical void volume is $0.419 \times 10^{-5} \text{ in}^3/\text{void}$ and the spherical void area is $0.00126 \text{ in}^2/\text{void}$. There are 11.83 times as many voids and the total void surface area is $43.3 \text{ in}^2/\text{in}^3 + 6.4 = 49.7 \text{ in}^2/\text{in}^3$, including perforations.

Therefore, the total initial burning surface area per in^3 of propellant is bounded by 78.5 in^2 as an absolute maximum, when all individual element surfaces are involved, and an area between 25 and $50 \text{ in}^2/\text{in}^3$. If perforations are not immediately ignited, these numbers are reduced to about $20\text{-}45 \text{ in}^2/\text{in}^3$. These limits essentially support the results generated by the one-dimensional flame spread and closed bomb experiments.

INITIAL DISTRIBUTION

HQ USAF/RDQRM	1	AFATL/DLDG	1
HQ USAF/SAMI	1	AFIS/INTA	1
HQ USAF/XOXFCM	1	ARADCOM/CODE SARPA	2
AFSC/IGFG	1	NAV SEA SYS CMD/CODE SEA-0332	1
AFSC/SDZA	1	NAV SEA SYS CMD/CODE SEA-992E	1
AFSC/DLCAW	1	NSWC/NAV ORD LAB	2
AFWL/DO/AMIC	1	OGDEN ALC/MMWRA	2
ASD/ENFEA	1	AFLC/MMMC	1
TAC/DRA	1	ASD/ENESS	1
AFWL/LR	1	AFATL/DLJ	2
AJL/AJL-LSE-70-239	1	AFATL/DLA	1
USA WPNS CMD SAPTR-LW-A	1	ADTC/SDC	1
USA Bal Resrch Lab DRXBR-TE	1	HQ USAFE/DOQ	1
Frankford Arsenal	1	HQ PACAF/DOO	1
Picatinny Arsenal	1	ASD/XRF	1
NAV WPNS CNTR CODE 31	1	TAC/INA	1
AF WPNS LAB/Tech Lib	1	AFATL/DLODR	1
NAV AIR SYS CMD/CODE AIR-5323	1	USATRADOCSYS ANA ACT/ATAA-SL	1
OF NAV RESRCH/CODE 473	1	COMIPAC/I-232	1
INST DEFENSE ANALYSIS/Clas Lib	1		
DDC/TC	2		
USAFTFWC/TA	1		
NAV WPNS LAB	1		
WATERVLIET Arsenal	1		
OGDEN ALC/MMM	2		
AF SPEC COM CNTR/SUR	3		
DQ DEPT ARMY/DAMA-WSA	2		
SARPA-FR-S-A	1		
AEDC/ARO, Inc	1		
AMXSY-DS	1		
USA MAT CMD/AMCR-YN	1		
NAV WPNS EVAL FAC	1		
OF CHN NAV OPNS AIR WARFARE	1		
DIR NAV RESRCH LAB/CODE 2627	1		
CAL INST OF TECH PROP DIV	1		
HQ PACAF/LGWSE	4		
USAFTAWC/TX	1		
TAWC/TRADOCLO	1		
AFATL/DL	1		
AFATL/DLY	1		
AFATL/DLOU	1		
AFATL/DLODL	2		
AFATL/DLYV	1		
AFATL/DLDD	1		
AFATL/DLDA	1		
AFATL/DLDE	1		
AFATL/DLDT	1		